Supporting Information

Methyl-Induced Ring-Locking Strategy for Concentration-Independent MR-TADF Emitters toward High-Performance OLEDs with BT. 2020 Blue Gamut

Gaoyu Li[a†], Yuyuan Wang[a†], Bo Wu[b], Jinkun Bian[a], Haozhi Xie[a], Zhiwei Ma[a], Hui Dai[a], Zhan Yang[*b], Xiangyu Ge[*c], Zhenguo Chi[*b]

[a] Guangdong Engineering Technology Research Center for High-performance Organic and Polymer Photoelectric Functional Films State Key Laboratory of Optoelectronic Material and Technologies, School of Chemistry Sun Yat-sen University, Guangzhou 510275, China

[b] School of Environmental and Chemical Engineering Wuyi University, Jiangmen 529020, China

[c] Key Laboratory of Guangdong Higher Education Institutions of Northeast Guangdong New Functional Materials, School of Chemistry and Environment, Jiaying University, Meizhou, 514015, Guangdong, P.R. China

*Corresponding Author(s): Zhan Yang: yangzhan@wyu.edu.cn; Xiangyu Ge: gexy28@mail.sysu.edu.cn; Zhenguo Chi: chizhg@mail.sysu.edu.cn

† Gaoyu Li and Yuyuan Wang contributed equally to this work.

Photophysical Characterization and Rate Constants Analysis

UV-visible absorption spectra were measured using a Hitachi U-3900 spectrophotometer at 298 K. PL spectra were recorded on a Shimadzu RF-5301PC spectrometer at both 298 K and 77 K. Doped films were prepared via vacuum deposition for the subsequent characterization PLQYs and transient PL decay properties. Absolute PLQYs were determined using a Quantaurus-QY measurement system (C11347-11, Hamamatsu Photonics). Transient PL decay curves of the doped films were acquired using an Edinburgh FLS 1000 spectrometer. Rate constants of different kinetic processes were calculated following the equations (1) - (6) below [1]:

$$k_p = \frac{1}{\tau_p} \tag{1}$$

$$k_d = \frac{1}{\tau_d} \tag{2}$$

$$k_r = \Phi_p k_p + \Phi_d k_d \approx \Phi_p k_p \tag{3}$$

$$k_{nr} = \frac{1 - \Phi_{PL}}{\Phi_{PL}} k_r \tag{4}$$

$$k_{ISC} = k_p - k_r - k_{nr} \tag{5}$$

$$k_{RISC} = (k_p k_d \Phi_d)/(k_{ISC} \Phi_p) \tag{6}$$

Where k_p, k_d, k_r, k_{nr}, k_{ISC}, k_{RISC} represent the rate constant of prompt fluorescence decay, delayed fluorescence decay, radiation, non-radiation, intersystem crossing and reverse intersystem crossing, respectively; Φ_{PL}, Φ_p, Φ_d, τ_p and τ_d represent total PLQY, quantum yield of the prompt component, quantum yield of the delayed component, lifetimes of the prompt and delayed components, respectively.

Single-Crystal Structure

Single-crystal X-ray data were determined using a Bruker APEX-II CCD X-ray Single Crystal Diffractometer with a (GaK\α) X-ray source, and single crystals were obtained via slow evaporation of CH_2Cl_2/*n*-Hex mixed solvents (CCDC numbers of 1M-BN, 2M-BN, 3M-BN and 4M-BN are 2525523, 2525524, 2525526, and 2525527 respectively).

Thermal and Electrochemical Characterization

Differential scanning calorimetry (DSC) measurements were carried out using a NETZSCH DSC 214 instrument under a nitrogen atmosphere at a heating rate of 20 °C min^{-1}. Thermogravimetric analyses (TGA) were performed on a NETZSCH TG 209F1 Libra analyzer under the same conditions. Cyclic voltammetry (CV) was conducted on a Bio-Logic VMP300 electrochemical workstation. At a scan rate of 100 mV s^{-1}, the oxidation/reduction potentials were measured in dry dichloromethane solutions with 0.1 M $TBAPF_6$ (tetrabutylammonium hexafluorophosphate) as a supporting electrolyte. HOMO = −4.8 − (E_{ox}−$E_{1/2(Ferrocene)}$), LUMO = HOMO + E_g. Where E_{ox} represents the onset oxidation potentials, $E_{1/2(Ferrocene)}$ represents the oxidation potential of ferrocene (F_c/F_{c+}), E_g represent optical bandgap obtained from the absorption onset.

Device Fabrication and Measurement

The indium tin oxide (ITO) substrates were carefully cleaned with 5% decon water, deionized water, acetone and isopropyl alcohol in sequence, and then dried. Before device preparation, the ITO substrates were pretreated with a Harrick Plasma surface cleaner. At vacuum pressure lower than 4×10^{-4} Pa, organic materials and metal layers were deposited sequentially on the ITO

substrates. The current density-voltage-luminance (J-V-L) characteristics were measured using a Topcon-SR-UL1R and a Keithley 2400 source.

Quantum Chemical Calculations

Theoretical chemical calculations were performed using the Gaussian 16 program package. Geometry optimizations of the molecules were carried out at the B3LYP-D3(BJ)/6-31G(d,p) level of density functional theory (DFT). The HOMO and LUMO energy levels were obtained based on these optimized geometries. The wave function analysis was carried out by using Multiwfn 3.8 program.[2,3] The SOC matrix elements were evaluated at the M062X-D3/def2SVP level using ORCA. The singlet and triplet energy levels were obtained based on SCS-CC2/cc-pVDZ level using the MRCC program.[4] Huang-Rhys factor and reorganization energy analyses were performed by the MOMAP (Molecular Materials Property Prediction Package).

Synthesis

$^{1}H/^{13}C$ NMR spectra were measured using a Bruker AvanceIII 400HD spectrometer, with deuterated dichloromethane (CD_2Cl_2) as solvent and tetramethylsilane (TMS) as an internal reference. High resolution mass spectra (HRMS) were collected from Agilent 6546 LC/Q-TOF spectrometer. Elemental analyses were measured by Elementar Vario EL Cube CHNS elemental analyzer.

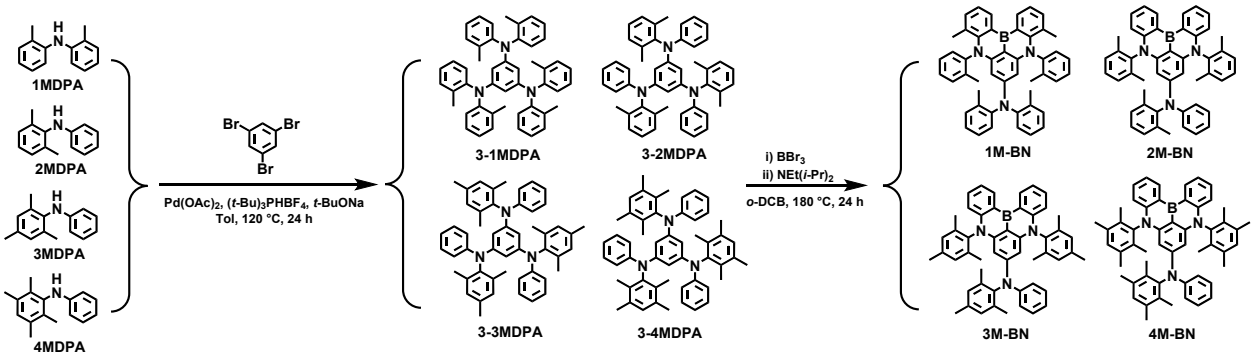

Scheme S1. Synthetic routes.

3-1MDPA: A mixture of 1,3,5-Tribromobenzene (1.00 g, 3.18 mmol), 1MDPA (1.94 g, 9.85 mmol) $Pd(OAc)_2$ (0.07 g, 0.32 mmol), *t*-Bu_3P (1M in Tol., 1 mL) and *t*-BuONa (2.75 g, 28.59 mmol) in 60 mL dry toluene were stirred at 120 °C for 24 h under argon. After cooling to room temperature, the crude product was extracted with dichloromethane. The organic phase was collected and dried with anhydrous sodium sulfate, and then the solvent was removed by distillation under reduced pressure. The residue was purified by column chromatography on silica gel using dichloromethane/ *n*-hexane (v/v = 7/93) as the eluent to afford the product as a white solid (1.83 g, yield: 86.8%) was obtained as white solid. ^{1}H NMR (600 MHz, CD_2Cl_2) δ 7.04 (d, *J* = 7.4 Hz, 6H), 6.99 (t, *J* = 6.8 Hz, 6H), 6.92 (t, *J* = 7.4 Hz, 6H), 6.80 (d, *J* = 8.2 Hz, 6H), 5.56 (s, 3H), 1.97 (s, 18H). ^{13}C NMR (151 MHz, CD_2Cl_2) δ 150.76, 146.83, 134.88, 131.89, 127.26, 126.97, 124.71, 108.13, 19.15.

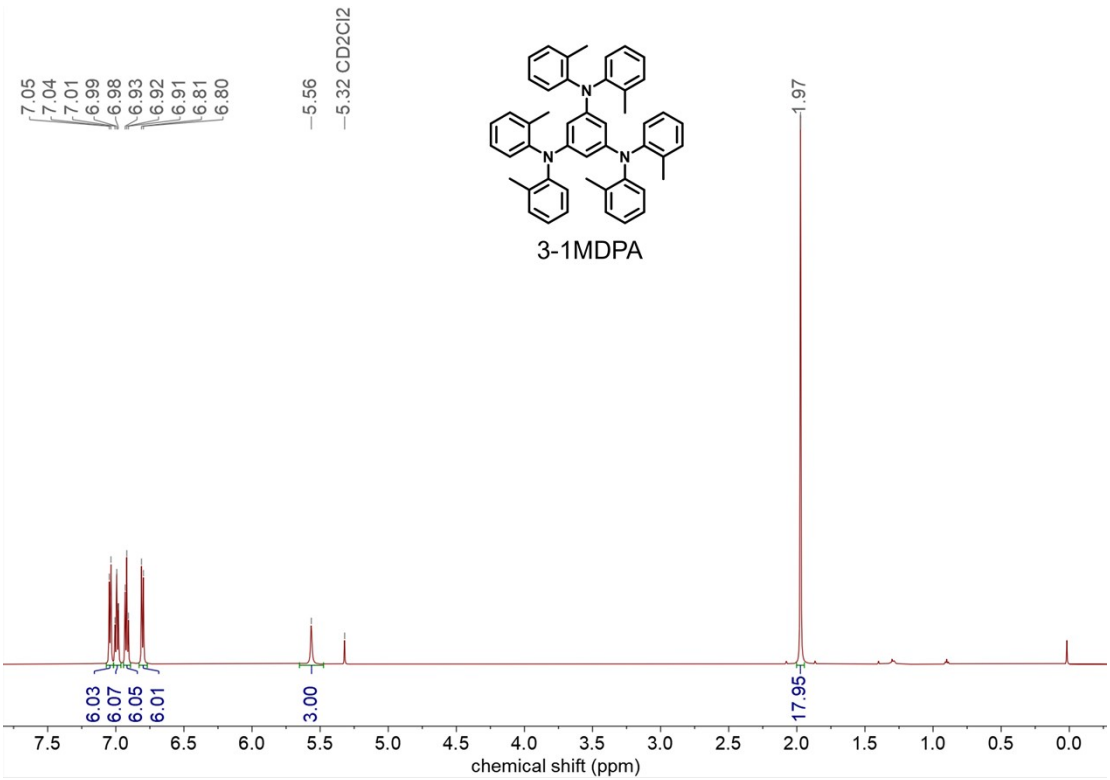

Figure S1. ^{1}H NMR spectrum of 3-1MDPA.

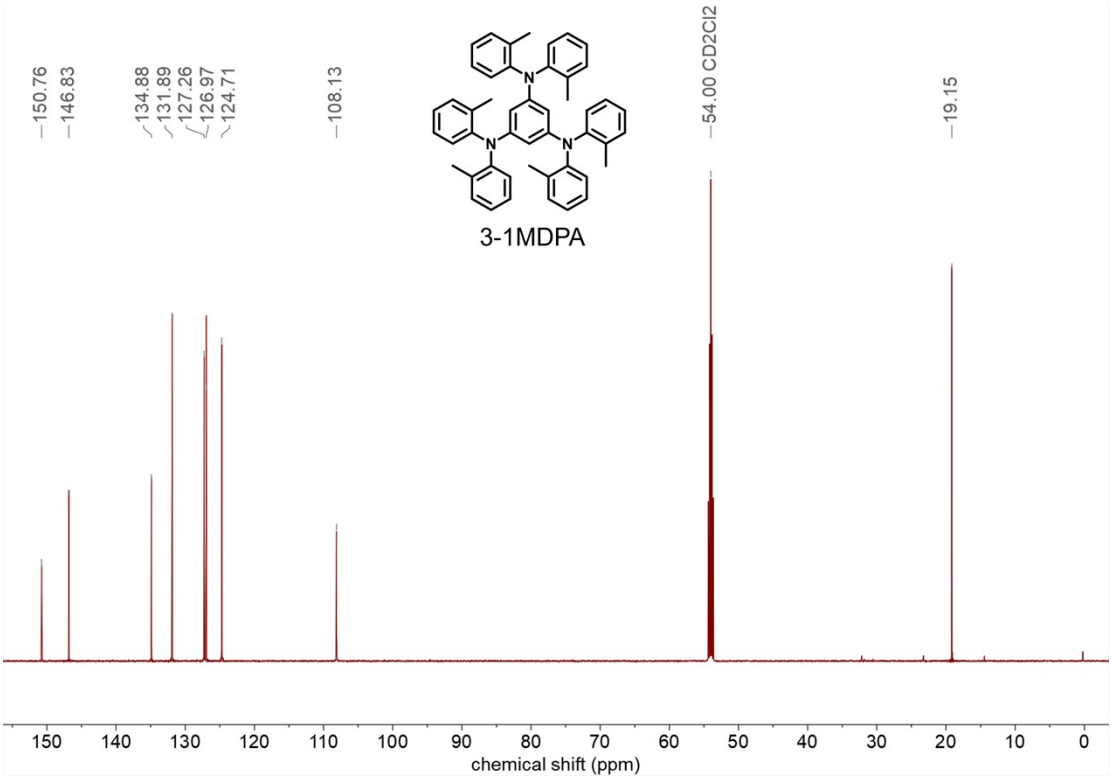

Figure S2. ^{13}C NMR spectrum of 3-1MDPA.

3-2MDPA: 3-2MDPA was synthesized according to the same procedure as 3-1MDPA by using 1,3,5-Tribromobenzene (1.00 g, 3.18 mmol), 2MDPA (1.94 g, 9.85 mmol) $Pd(OAc)_2$ (0.07 g, 0.32 mmol), *t*-Bu_3P (1M in Tol., 1 mL) and *t*-BuONa (2.75 g, 28.59 mmol). 3-2MDPA (1.93 g, yield: 92%) was obtained as white solid. ^{1}H NMR (600 MHz, CD_2Cl_2) δ 7.11-7.07 (m, 6H), 7.06 (dd, *J* = 8.2, 6.5 Hz, 3H), 7.00 (d, *J* = 7.5 Hz, 6H), 6.83 (d, *J* = 7.5 Hz, 6H), 6.77 (t, *J* = 7.3 Hz, 3H), 6.07 (s, 3H), 1.93 (s, 18H). ^{13}C NMR (151 MHz, CD_2Cl_2) δ 147.41, 146.32, 143.09, 138.32, 129.45, 129.32, 127.49, 120.83, 119.70, 105.34, 18.61.

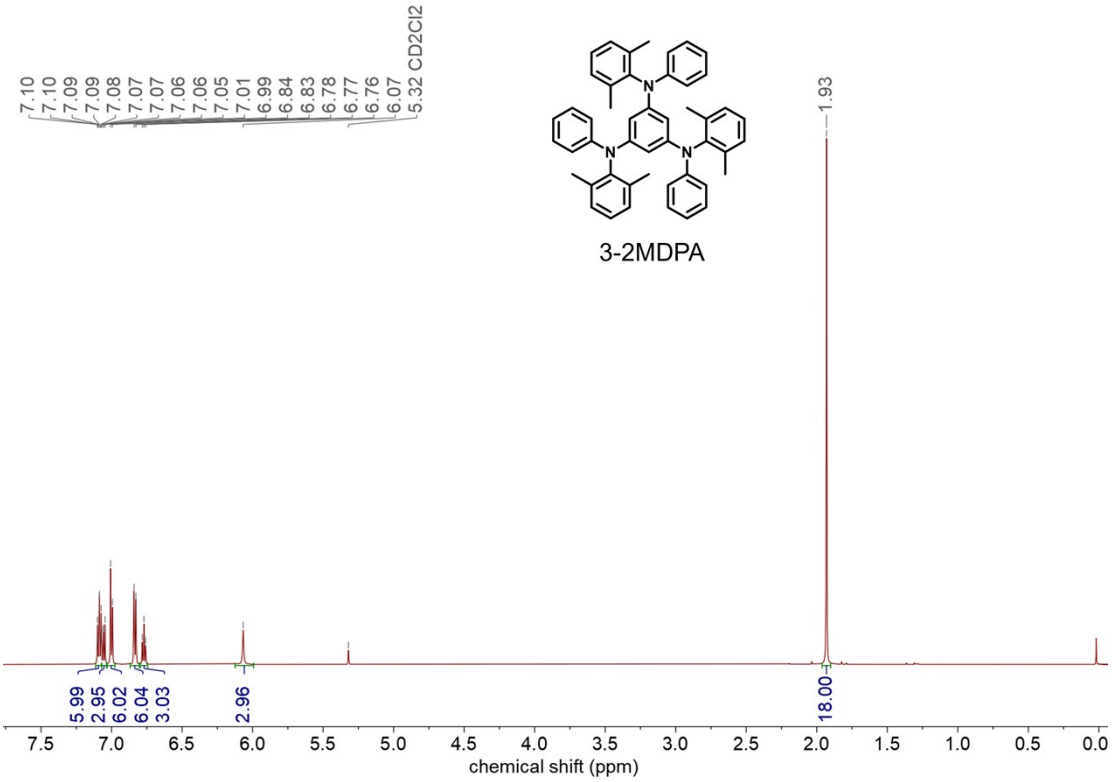

Figure S3. ^{1}H NMR spectrum of 3-2MDPA.

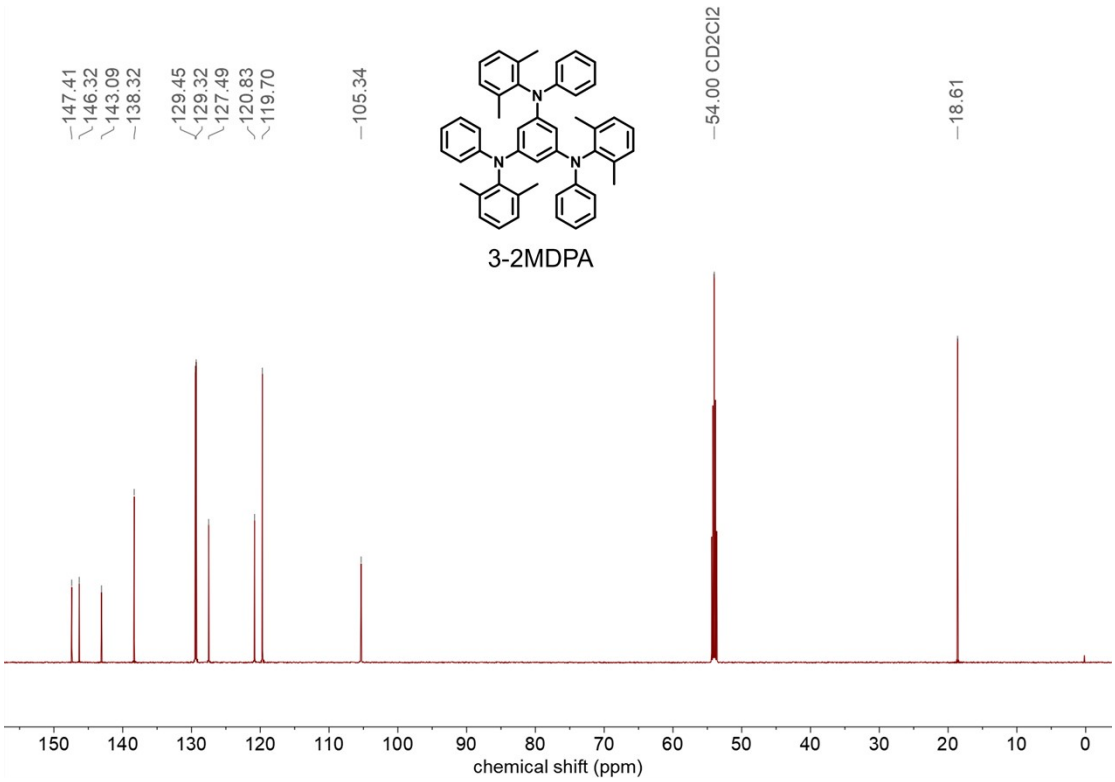

Figure S4. ^{13}C NMR spectrum of 3-2MDPA.

3-3MDPA: 3-3MDPA was synthesized according to the same procedure as 3-MDPA by using 1,3,5-Tribromobenzene (1.00 g, 3.18 mmol), 3MDPA (2.08 g, 9.85 mmol) $Pd(OAc)_2$ (0.07 g, 0.32 mmol), *t*-Bu_3P (1M in Tol., 1 mL) and *t*-BuONa (2.75 g, 28.59 mmol). 3-3MDPA (1.76 g, yield: 79%) was obtained as white solid. ^1H NMR (600 MHz, CD_2Cl_2) δ 7.11-7.02 (m, 6H), 6.85 (d, *J* = 8.6 Hz, 6H), 6.81 (s, 5H), 6.76 (t, *J* = 7.2 Hz, 4H), 6.04 (s, 3H), 2.27 (s, 9H), 1.88 (s, 18H). ^{13}C NMR (151 MHz, CD_2Cl_2) δ 147.40, 146.50, 140.53, 137.90, 137.11, 130.04, 129.27, 120.64, 119.63, 105.09, 21.27, 18.48.

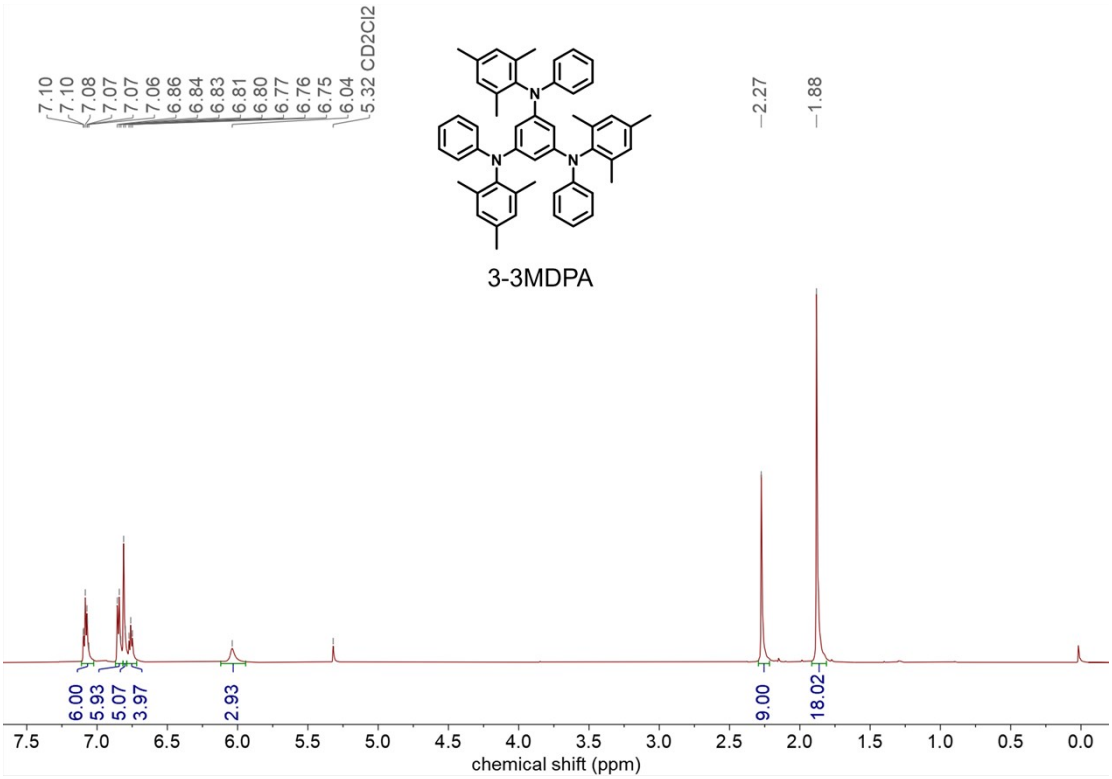

Figure S5. ^{1}H NMR spectrum of 3-3MDPA.

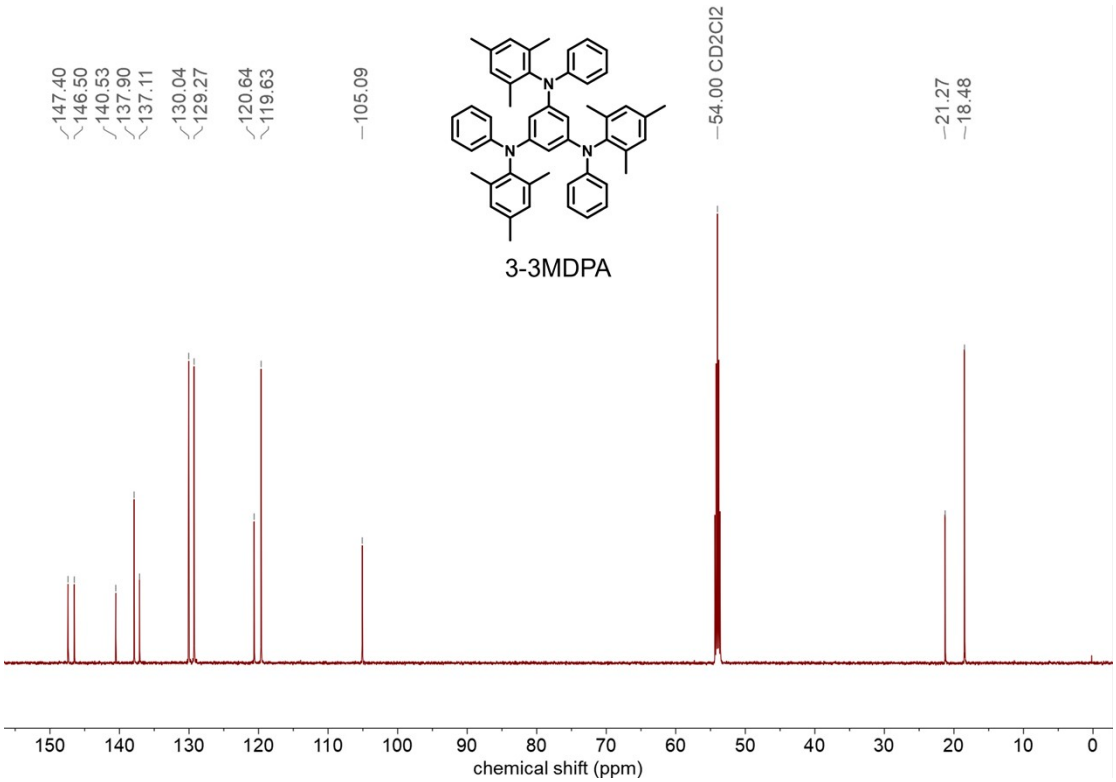

Figure S6. ^{13}C NMR spectrum of 3-3MDPA.

3-4MDPA: 3-4MDPA was synthesized according to the same procedure as 3-1MDPA by using 1,3,5-Tribromobenzene (1.00 g, 3.18 mmol), 4MDPA (2.22 g, 9.85 mmol) $Pd(OAc)_2$ (0.07 g, 0.32 mmol), *t*-Bu_3P (1M in Tol., 1 mL) and *t*-BuONa (2.75 g, 28.59 mmol). 3-4MDPA (1.72 g, yield: 72.4%) was obtained as white solid. ^1H NMR (600 MHz, CD_2Cl_2) δ 7.09 (t, *J* = 7.5 Hz, 6H), 6.91-6.83 (m, 9H), 6.76 (t, *J* = 7.3 Hz, 3H), 5.97 (s, 3H), 2.15 (s, 18H), 1.80 (s, 18H). ^{13}C NMR (151 MHz, CD_2Cl_2) δ 147.31, 146.58, 142.92, 135.46, 133.98, 130.57, 129.21, 120.50, 119.58, 104.39, 20.31, 14.52.

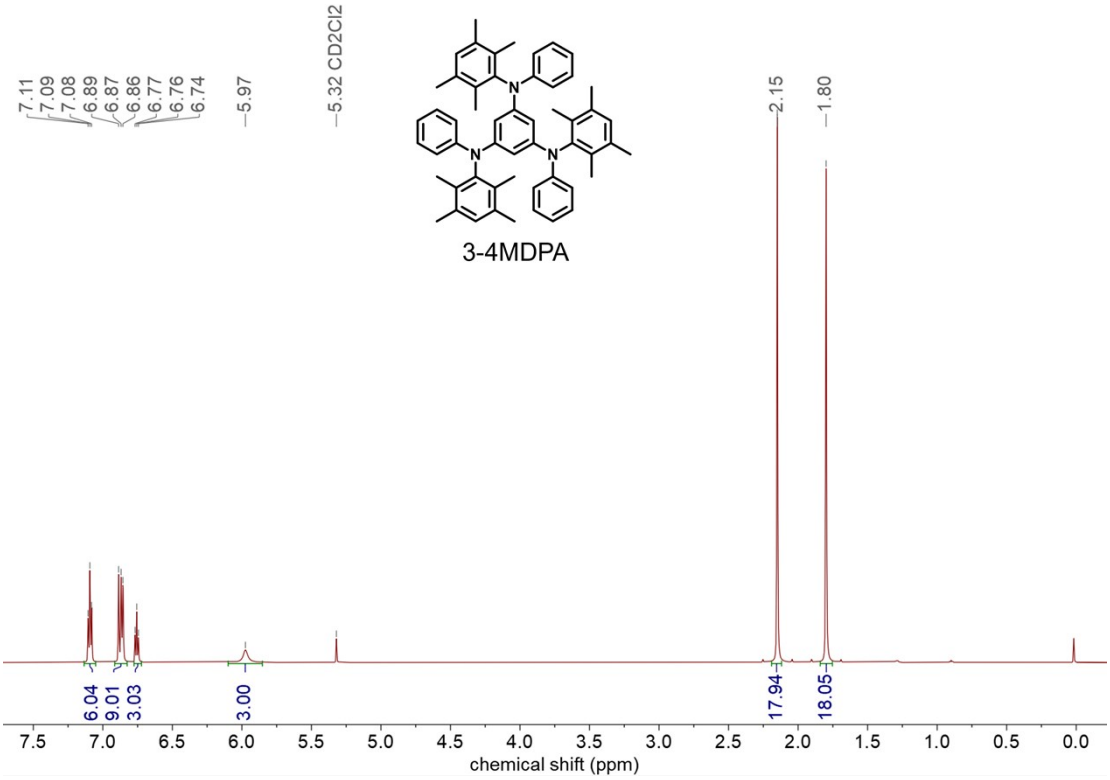

Figure S7. ^1H NMR spectrum of 3-4MDPA.

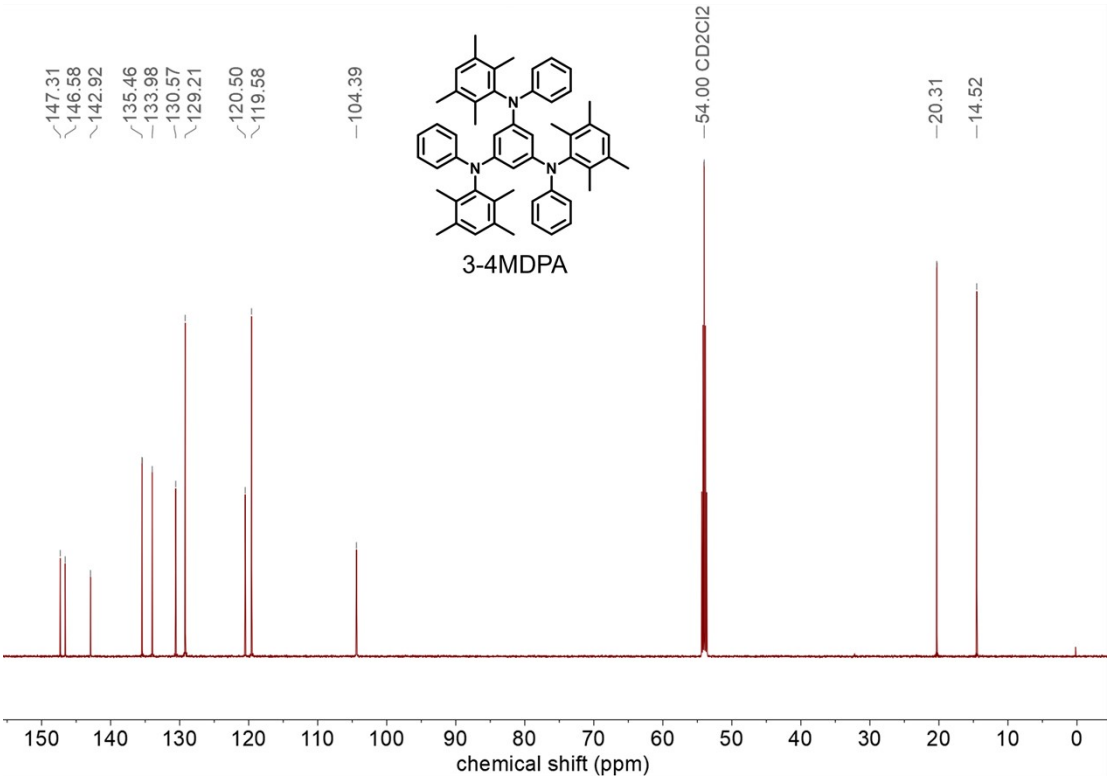

Figure S8. ^{13}C NMR spectrum of 3-4MDPA.

1M-BN: A solution of 3-1MDPA (1.70 g, 2.56 mmol) in dry o-dichlorobenzene solution (20 mL) was quickly added boron tribromide (3.85 g, 15.36 mmol) under argon atmosphere, and then stirred at 180 °C for 24 h. After cooling to 0 °C, the and *N,N*-diisopropylethylamine (3.97 g, 30.73 mmol) was added to quench the reaction, and the solvent in the crude product was removed by distillation under reduced pressure. The residue was purified by column chromatography on silica gel using dichloromethane/petroleum ether (v/v = 0 to 5/95) as the eluent to obtain the product as a yellow solid (1.27 g, yield: 74%). ^{1}H NMR (600 MHz, CD_2Cl_2) δ 8.54 (d, *J* = 7.5 Hz, 2H), 7.24 (d, *J* = 7.2 Hz, 2H), 7.16 (t, *J* = 7.5 Hz, 2H), 7.13 (t, *J* = 6.8 Hz, 3H), 7.07 (t, *J* = 6.9 Hz, 4H), 7.05 – 6.97 (m, 7H), 6.81 (q, *J* = 4.4 Hz, 2H), 5.40 (s, 2H), 1.93 (s, 3H), 1.84 (d, *J* = 7.6 Hz, 9H), 1.67 (s, 6H). ^{13}C NMR (151 MHz, CD_2Cl_2) δ 152.89, 148.98, 147.93, 147.76, 145.16, 144.82, 138.94, 138.85, 136.45, 135.77, 133.97, 133.92, 132.10, 131.93, 131.55, 131.37, 131.27, 128.41, 128.36, 128.29, 127.31, 127.19, 127.05, 125.95, 125.80, 120.79, 96.82, 54.36, 54.18, 54.00, 53.82, 53.64, 24.27, 23.99,

18.83, 18.29, 18.11. HRMS (ESI): *m/z*, $[M + H]^+$ calcd for $C_{48}H_{42}BN_3$: 672.3545, found: 672.3555.

Anal. Calcd for: C, 85.83; H, 6.30; N, 6.26. found C, 85.74; H, 6.56; N, 6.08.

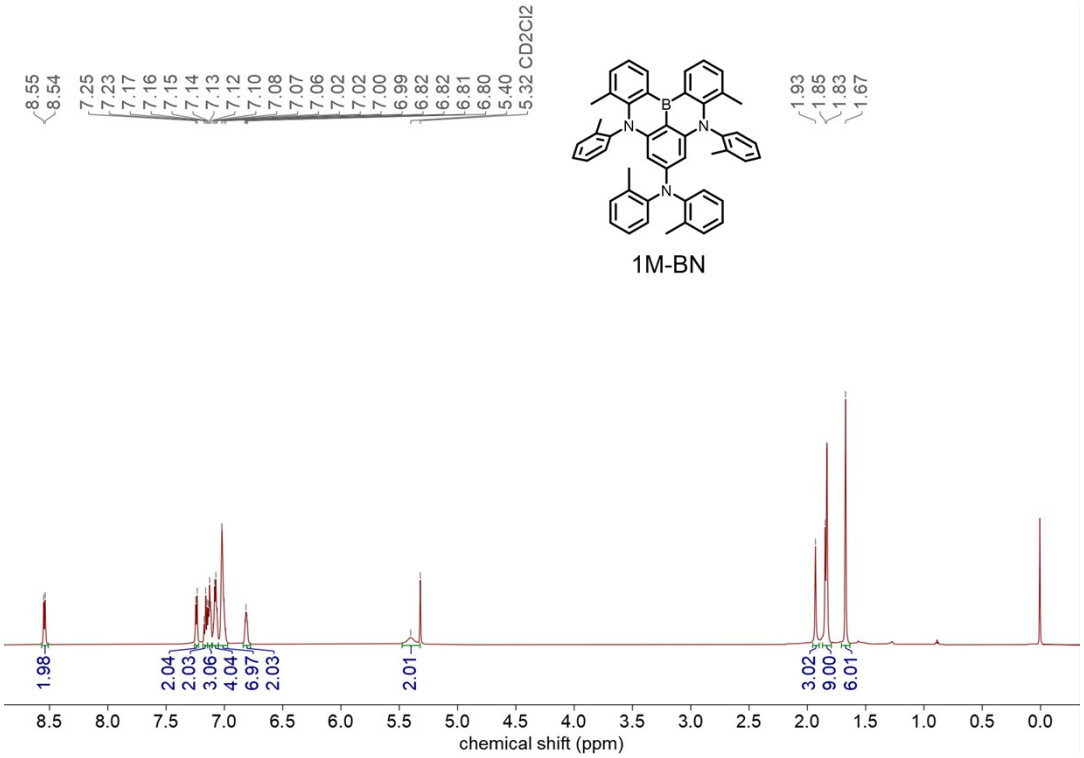

Figure S9. ^{1}H NMR spectrum of 1M-BN.

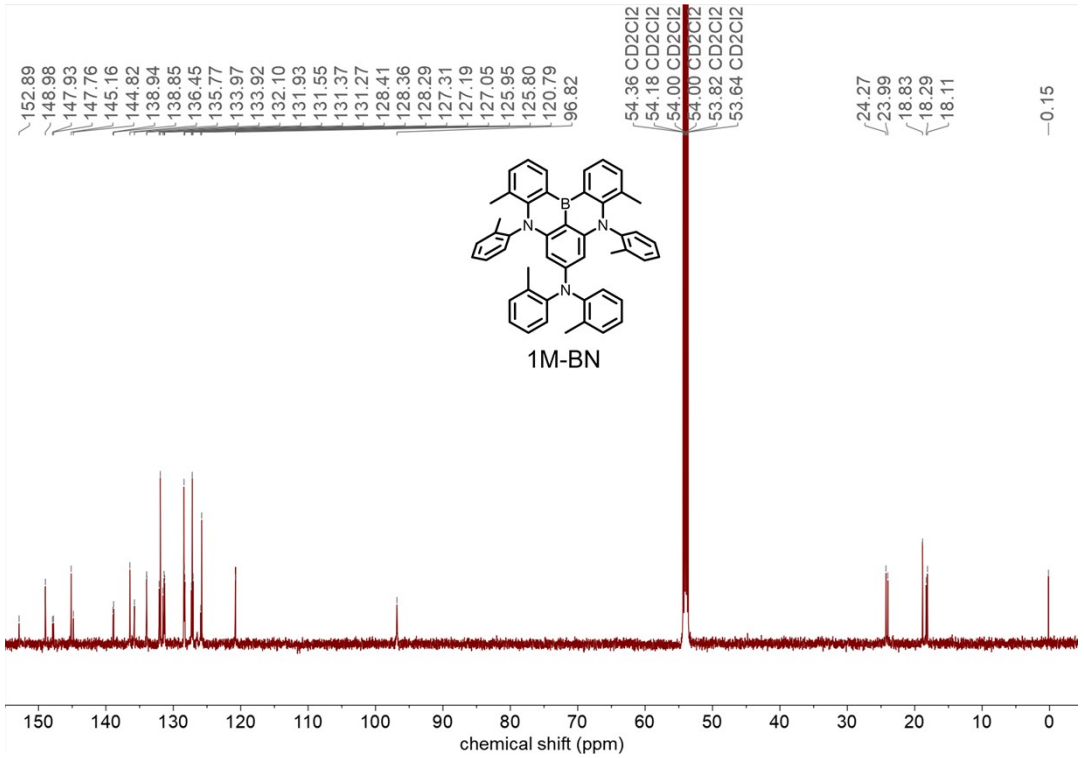

Figure S10. ^{13}C NMR spectrum of 1M-BN.

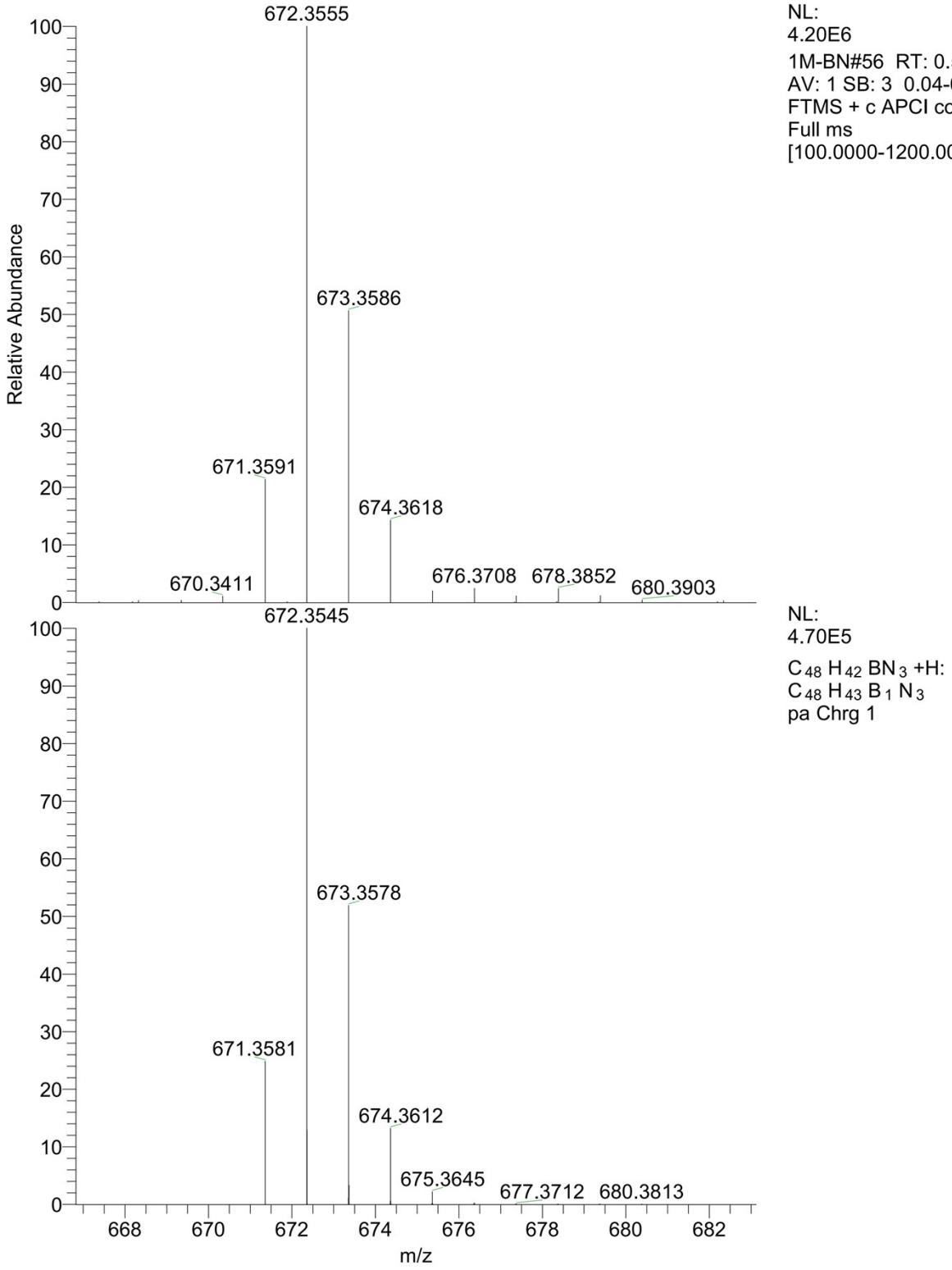

Figure S11. HRMS spectrum of 1M-BN.

2M-BN: 2M-BN was synthesized according to the same procedure as 1M-BN by using 3-2MDPA (1.70 g, 2.56 mmol), boron tribromide (3.85 g, 15.36 mmol) and *N,N*-diisopropylethylamine (3.97 g, 30.73 mmol). 2M-BN (1.53 g, yield: 79.7%) was obtained as yellow solid. ^{1}H NMR (600 MHz, CD_2Cl_2) δ 8.95 (d, *J* = 7.6 Hz, 2H), 7.41-7.37 (m, 2H), 7.23 (dd, *J* = 16.0, 8.2 Hz, 4H), 7.17 (d, *J* = 7.6 Hz, 4H), 7.03 (t, *J* = 6.9 Hz, 3H), 6.91 (d, *J* = 7.6 Hz, 2H), 6.85 (d, *J* = 8.0 Hz, 2H), 6.78 (t, *J* = 7.3 Hz, 1H), 6.65 (d, *J* = 8.6 Hz, 2H), 5.57 (s, 2H), 1.84 (s, 12H), 1.78 (s, 6H). ^{13}C NMR (151 MHz, CD_2Cl_2) δ 150.96, 146.90, 146.51, 145.17, 142.96, 139.76, 138.15, 137.80, 135.49, 131.57, 129.83, 129.28, 129.05, 128.79, 127.72, 121.66, 120.41, 120.30, 115.67, 95.07, 18.23, 17.59. HRMS (ESI): *m/z*, $[M]^+$ calcd for $C_{48}H_{42}BN_3$: 672.3545, found: 672.3555. Anal. Calcd for: C, 85.83; H, 6.30; N, 6.26. found C, 85.75; H, 6.19; N, 6.14.

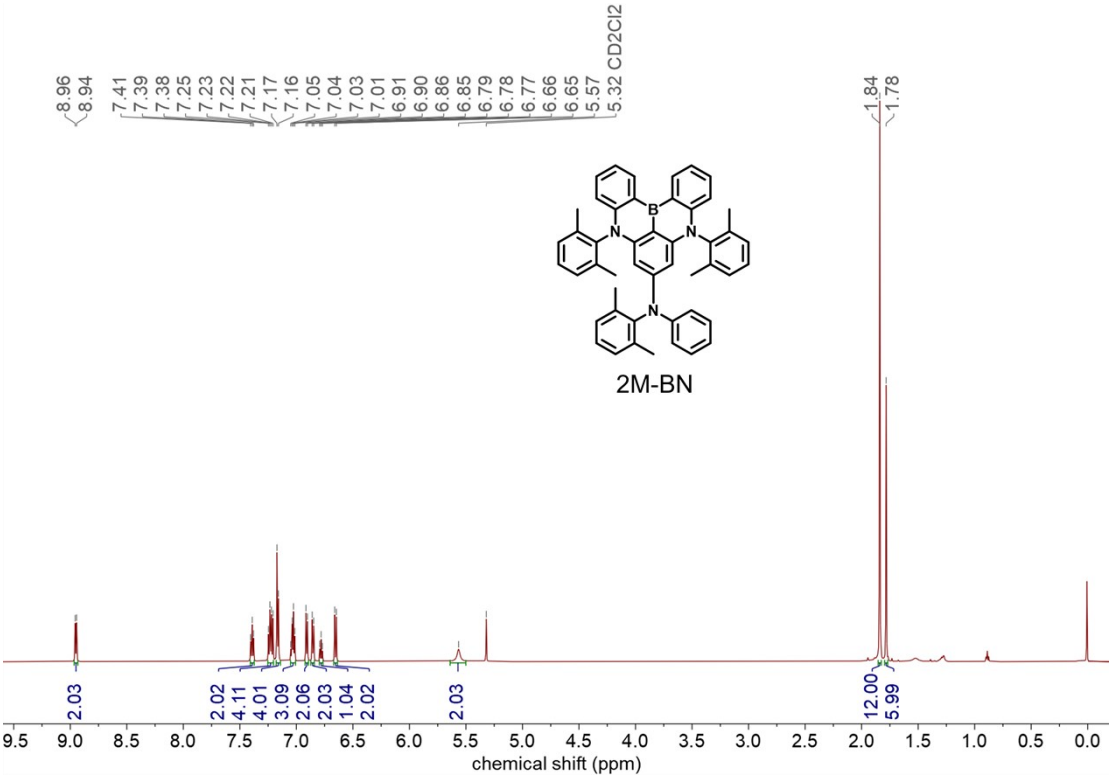

Figure S12. ^{1}H NMR spectrum of 2M-BN.

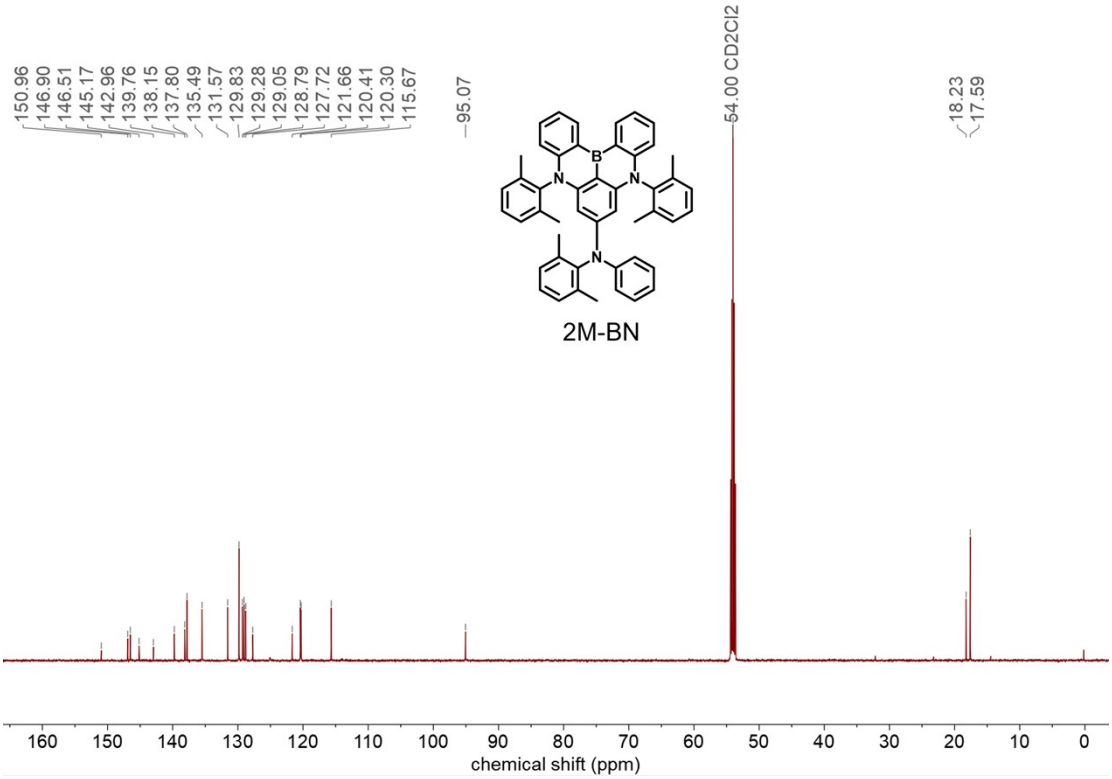

Figure S13. ^{13}C NMR spectrum of 2M-BN.

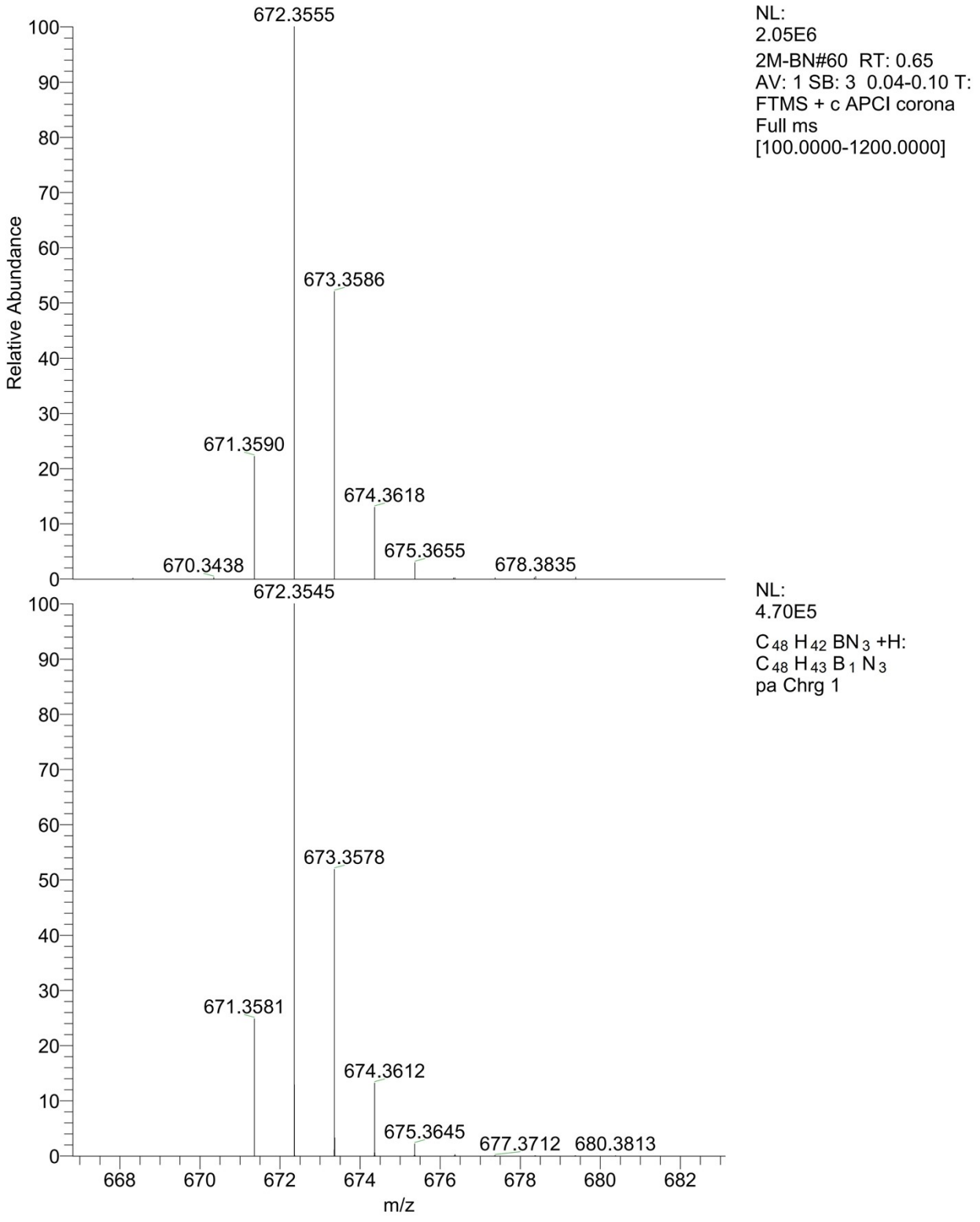

Figure S14. HRMS spectrum of 2M-BN.

3M-BN: 3M-BN was synthesized according to the same procedure as 1M-BN by using 3-3MDPA (1.50 g, 2.15 mmol), boron tribromide (3.23 g, 12.91 mmol) and *N,N*-diisopropylethylamine (3.34 g, 25.82 mmol). 3M-BN (1.13 g, yield: 74.5%) was obtained as yellow solid. ^{1}H NMR (600 MHz, CD_2Cl_2) δ 8.97 (d, *J* = 7.5 Hz, 2H), 7.45-7.39 (m, 2H), 7.28-7.23 (m, 2H), 7.09-7.04 (m, 2H), 7.02 (s, 4H), 6.91 (d, *J* = 7.5 Hz, 2H), 6.82 (t, *J* = 7.2 Hz, 1H), 6.78 (s, 2H), 6.74 (d, *J* = 8.6 Hz, 2H), 5.59 (s, 2H), 2.39 (s, 6H), 2.35 (s, 3H), 1.83 (s, 12H), 1.78 (s, 6H). ^{13}C NMR (151 MHz, CD_2Cl_2) δ 150.25, 146.46, 146.08, 144.61, 139.82, 137.94, 137.20, 136.75, 136.69, 136.58, 134.83, 130.84, 129.78, 129.17, 128.40, 120.94, 119.79, 119.53, 115.13, 94.18, 20.77, 20.72, 17.51, 16.92. HRMS (ESI): *m/z*, [M + H]$^{+}$ calcd for $C_{51}H_{48}BN_3$: 714.4014, found: 714.4024. Anal. Calcd for: C, 85.82; H, 6.78; N, 5.89. found C, 85.70; H, 7.08; N, 5.65.

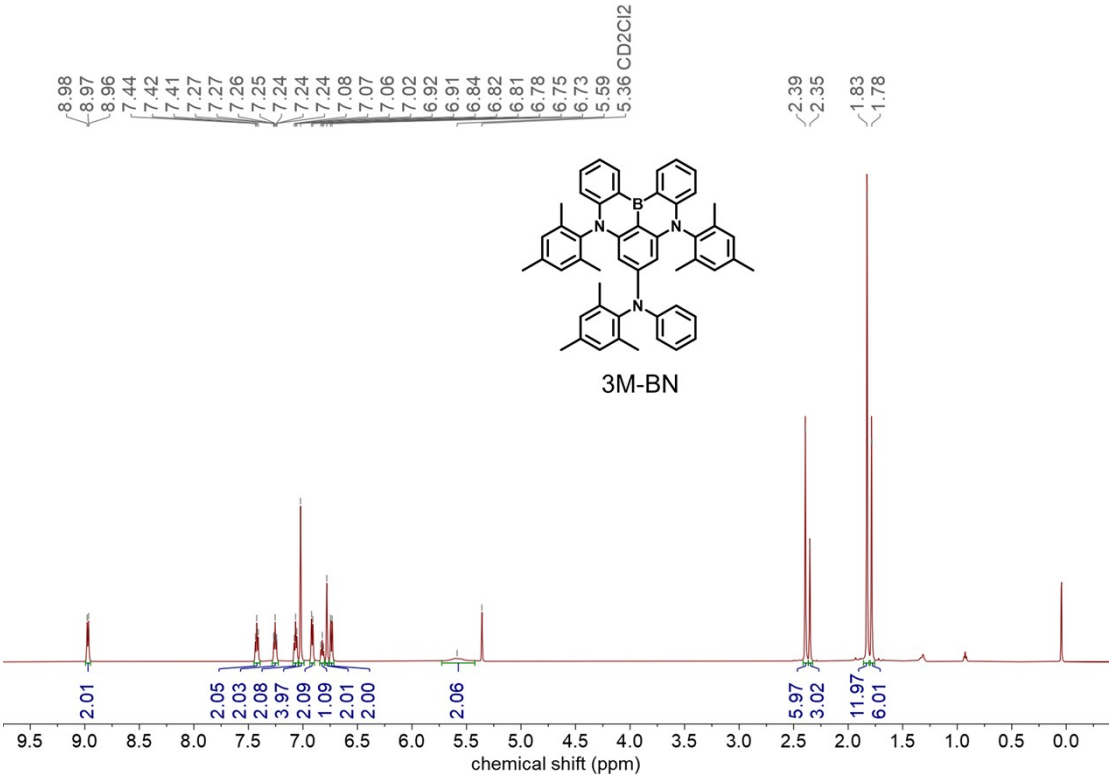

Figure S15. ^{1}H NMR spectrum of 3M-BN.

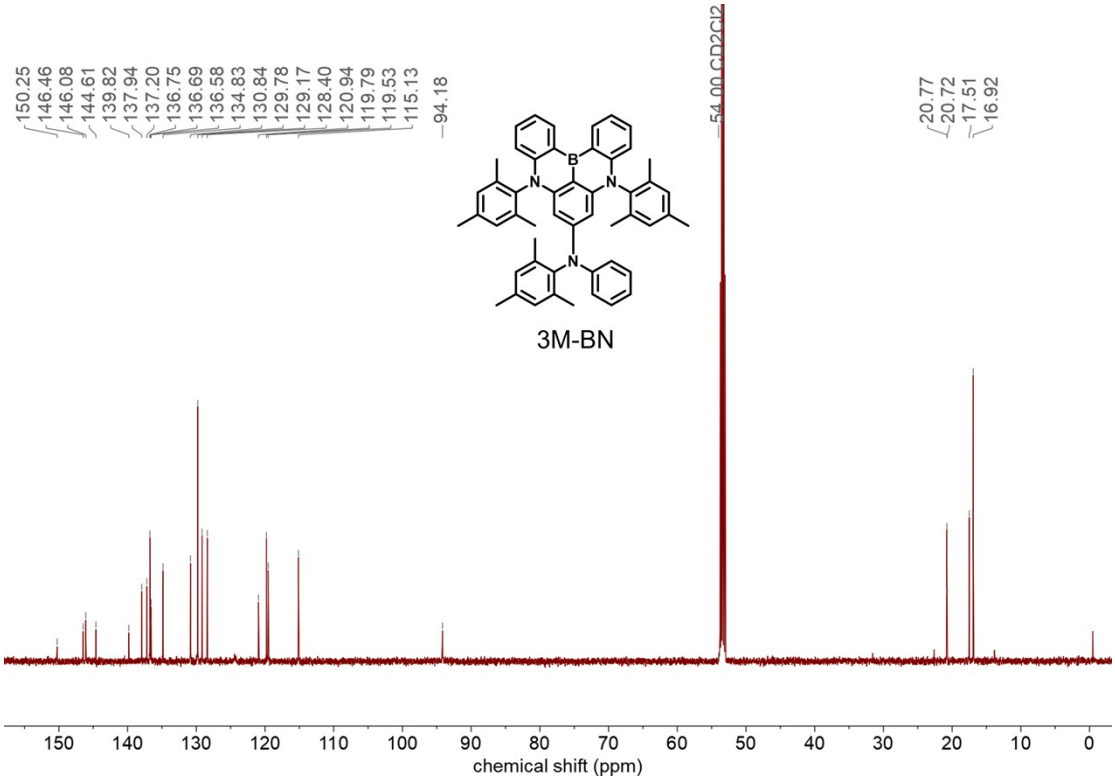

Figure S16. ^{13}C NMR spectrum of 3M-BN.

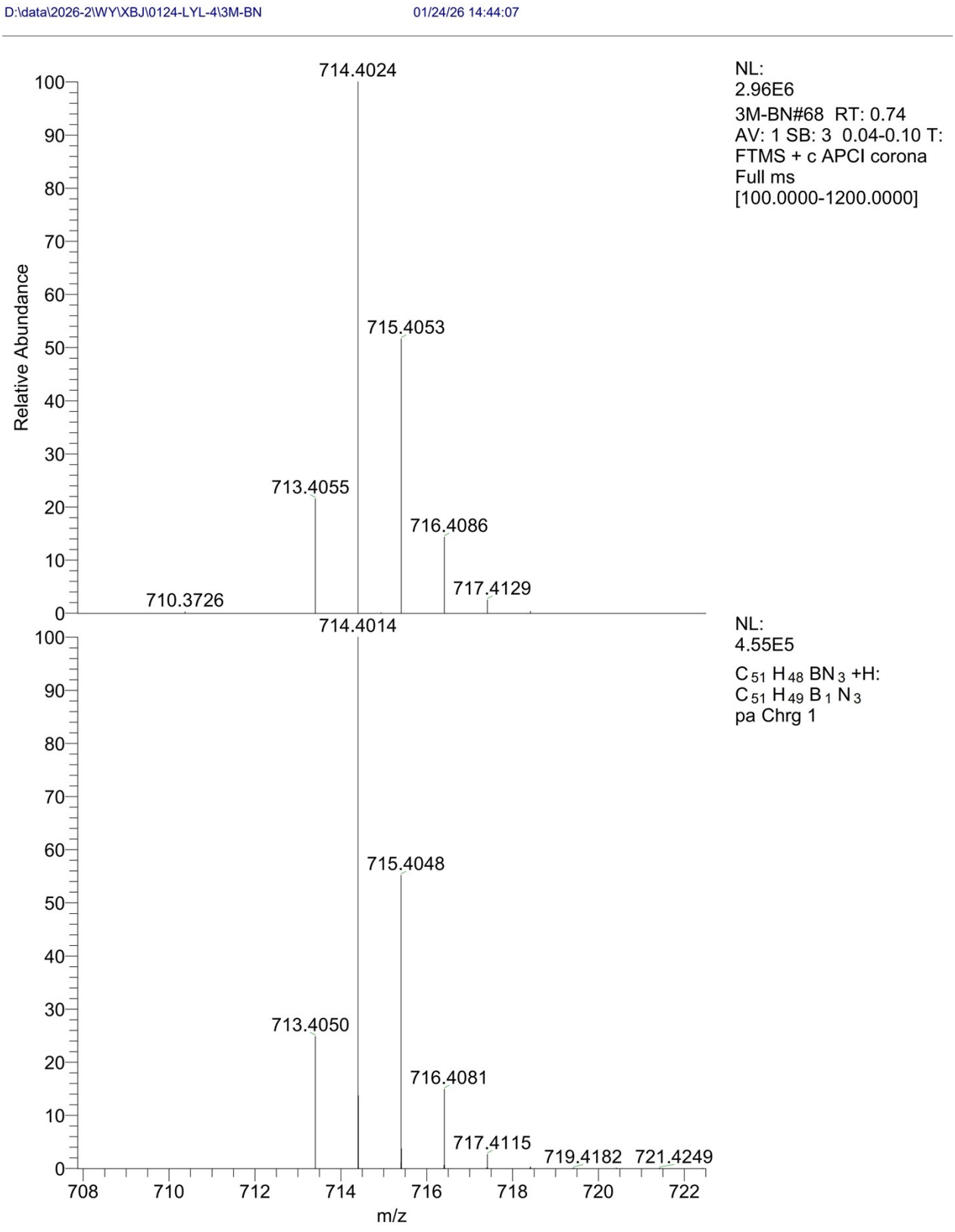

Figure S17. HRMS spectrum of 3M-BN.

4M-BN: 4M-BN was synthesized according to the same procedure as 1M-BN by using 3-4MDPA (1.40 g, 1.87 mmol), boron tribromide (2.81 g, 11.23 mmol) and *N,N*-diisopropylethylamine (2.91 g, 22.46 mmol). 4M-BN (0.94 g, yield: 66.5%) was obtained as yellow solid. ^{1}H NMR (600 MHz, CD_2Cl_2) δ 8.98 (d, *J* = 7.7 Hz, 2H), 7.41 (t, *J* = 7.8 Hz, 2H), 7.25 (t, *J* = 7.3 Hz, 2H), 7.08 (s, 2H), 7.06 (d, *J* = 7.9 Hz, 2H), 6.92-6.86 (m, 3H), 6.80 (t, *J* = 7.3 Hz, 1H), 6.68 (d, *J* = 8.6 Hz, 2H), 5.51 (s, 2H), 2.28 (s, 12H), 2.16 (s, 6H), 1.70 (d, *J* = 19.7 Hz, 18H). ^{13}C NMR (151 MHz, CD_2Cl_2) δ 150.51, 147.11, 146.92, 145.62, 142.84, 139.65, 136.17, 135.39, 135.30, 133.82, 133.14, 131.43, 131.32, 130.72, 128.83, 121.14, 120.08, 119.70, 116.18, 95.80, 20.31, 20.29, 14.18, 13.87. HRMS (ESI): *m/z*, $[M]^+$ calcd for $C_{54}H_{54}BN_3$: 755.4484, found: 755.4494. Anal. Calcd for: C, 85.81; H, 7.20; N, 5.56. found C, 85.94; H, 7.34; N, 5.40.

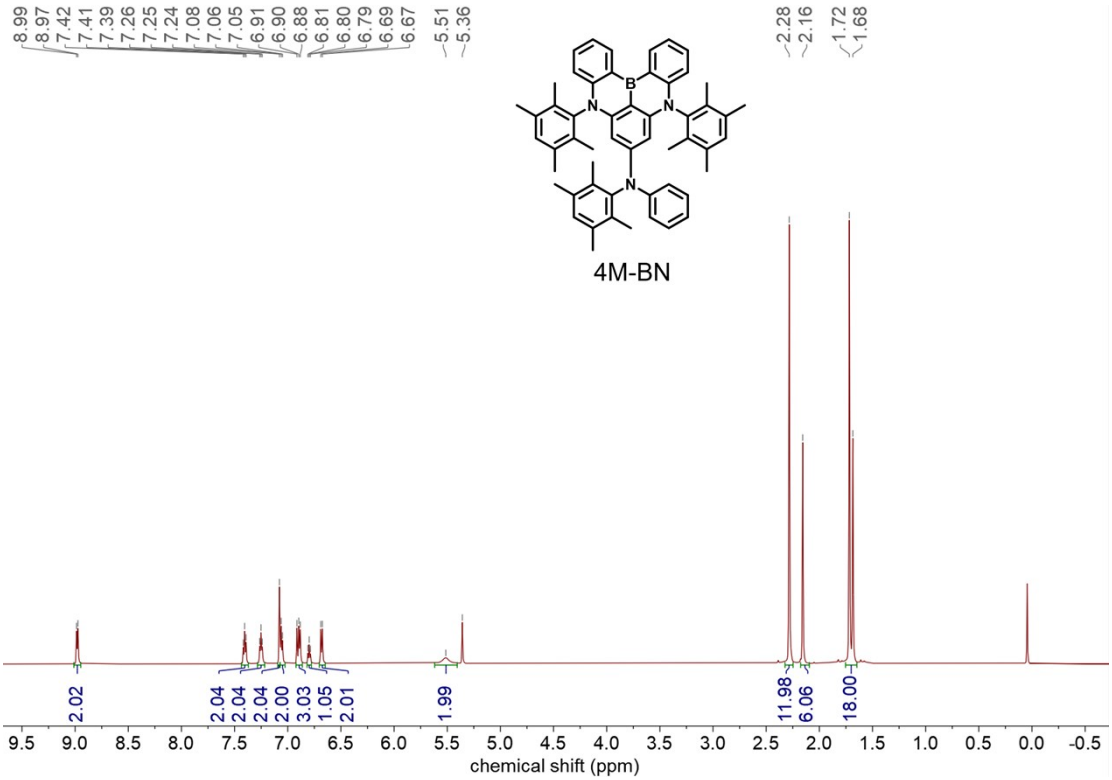

Figure S18. ^{1}H NMR spectrum of 4M-BN.

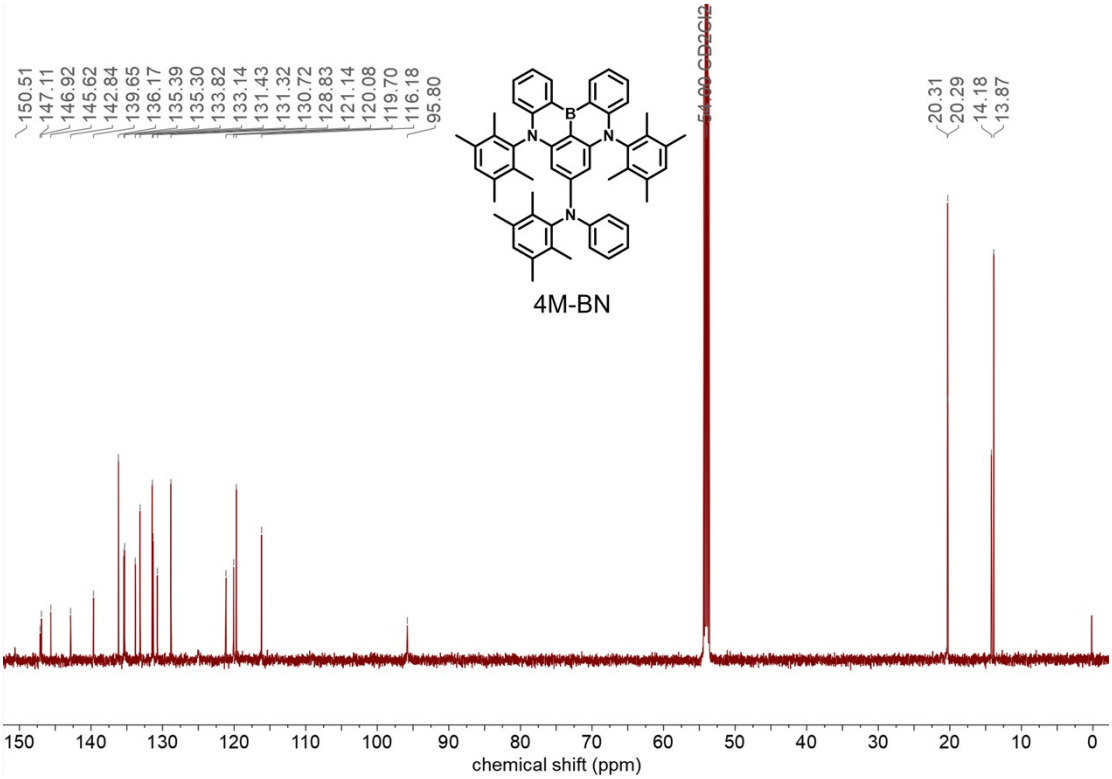

Figure S19. ^{13}C NMR spectrum of 4M-BN.

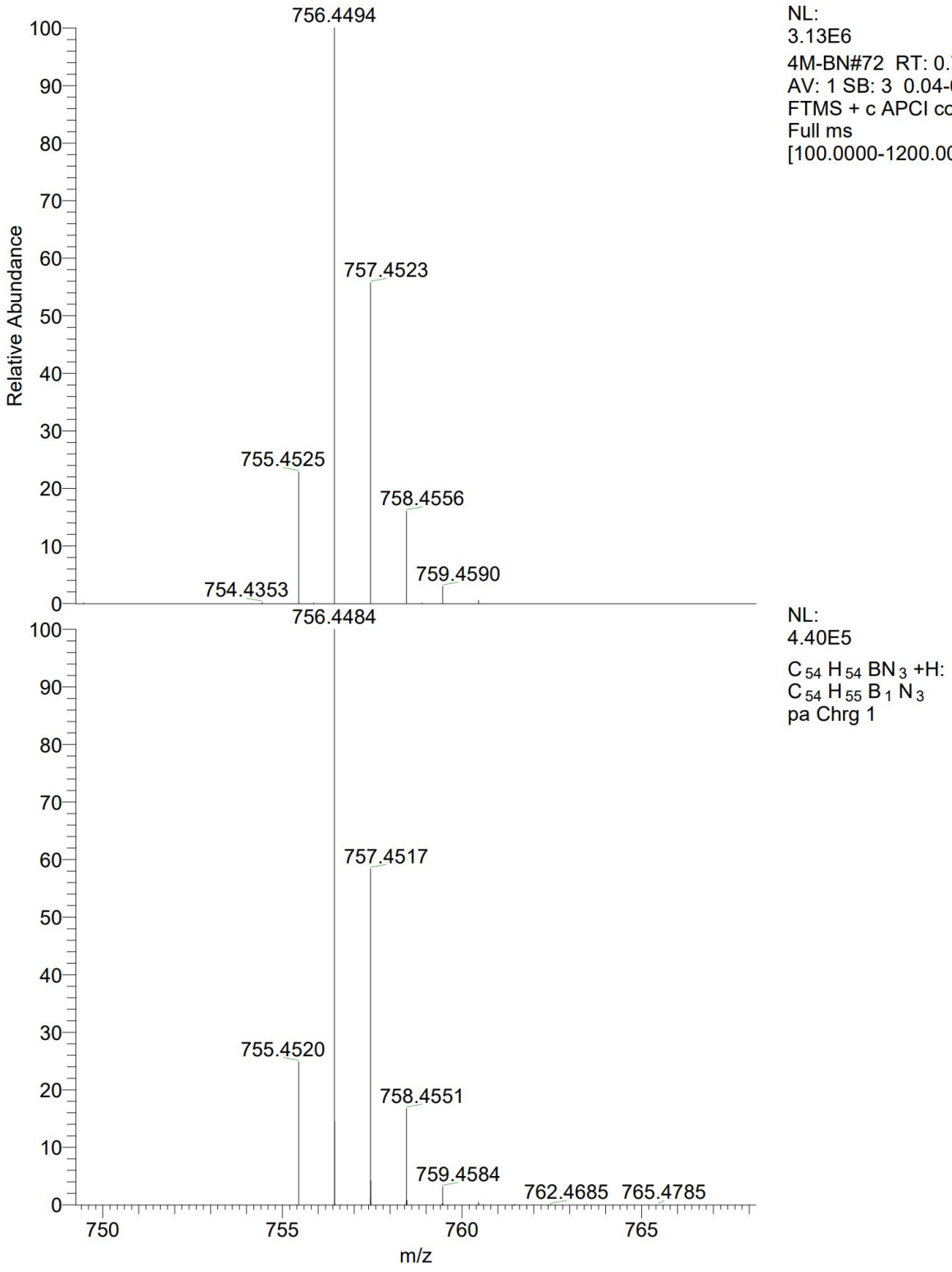

Figure S20. HRMS spectrum of 4M-BN.

CHN元素含量测定
vario EL cube 元素分析仪

Text report

No.	Memo	Name	Weight [mg]	Method	C [%]	H [%]	N [%]	C/N ratio	C/H ratio	Date Time
59	080687	1M-BN	1.517	2mg80s	86.51	6.70	6.17	14.019	12.916	02.04.2026 16:12
60		1M-BN	1.507	2mg80s	85.74	6.56	6.08	14.109	13.073	02.04.2026 16:20
61		2M-BN	1.557	2mg80s	85.32	6.53	6.13	13.912	13.056	02.04.2026 16:29
62		2M-BN	1.535	2mg80s	85.75	6.19	6.14	13.961	13.862	02.04.2026 16:37
63		3M-BN	1.474	2mg80s	86.02	7.17	5.67	15.171	11.999	02.04.2026 16:46
64		3M-BN	1.542	2mg80s	85.70	7.08	5.65	15.173	12.112	02.04.2026 16:54
65		4M-BN	1.524	2mg80s	86.09	7.39	5.42	15.886	11.649	02.04.2026 17:03
66		4M-BN	1.561	2mg80s	85.94	7.34	5.40	15.919	11.701	02.04.2026 17:11

Figure S21. Elemental analyses of 1M-BN, 2M-BN, 3M-BN and 4M-BN.

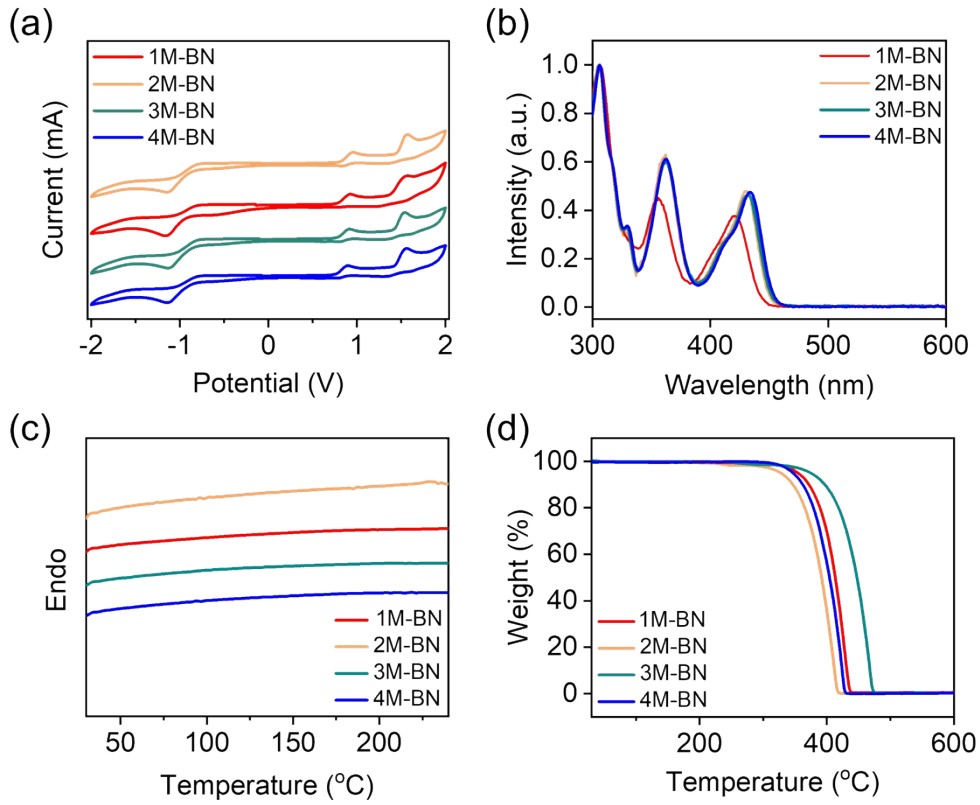

Figure S22. Cyclic voltammetry measurements (a), UV-vis absorption spectra in dichloromethane solvent (b), differential scanning calorimetry curves (c) and thermogravimetric analysis curves (d) of 1M-BN, 2M-BN, 3M-BN and 4M-BN.

Table S1. Electrochemical and thermal properties.

Com.	HOMO [eV]	LUMO [eV]	T_d [°C]
1M-BN	-5.24	-2.54	354.4
2M-BN	-5.27	-2.53	327.5
3M-BN	-5.25	-2.53	374.6
4M-BN	-5.23	-2.52	346.5

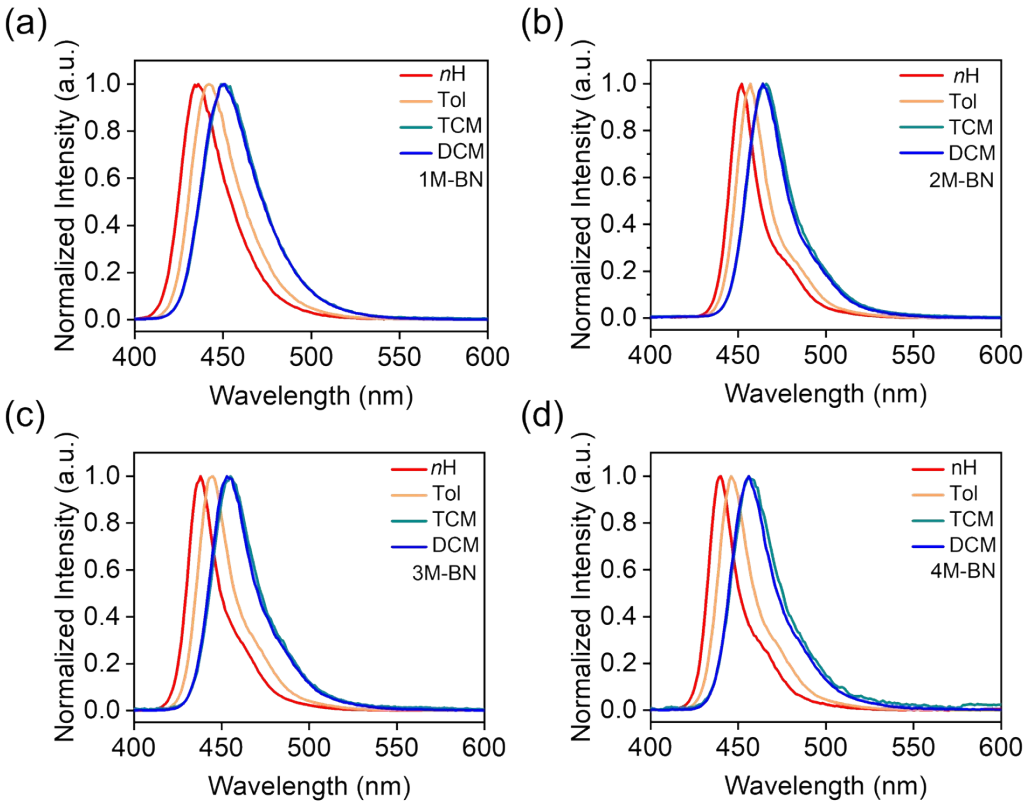

Figure S23. PL spectra of (a) 1M-BN, (b) 2M-BN, (c) 3M-BN and (d) 4M-BN in different solvents.

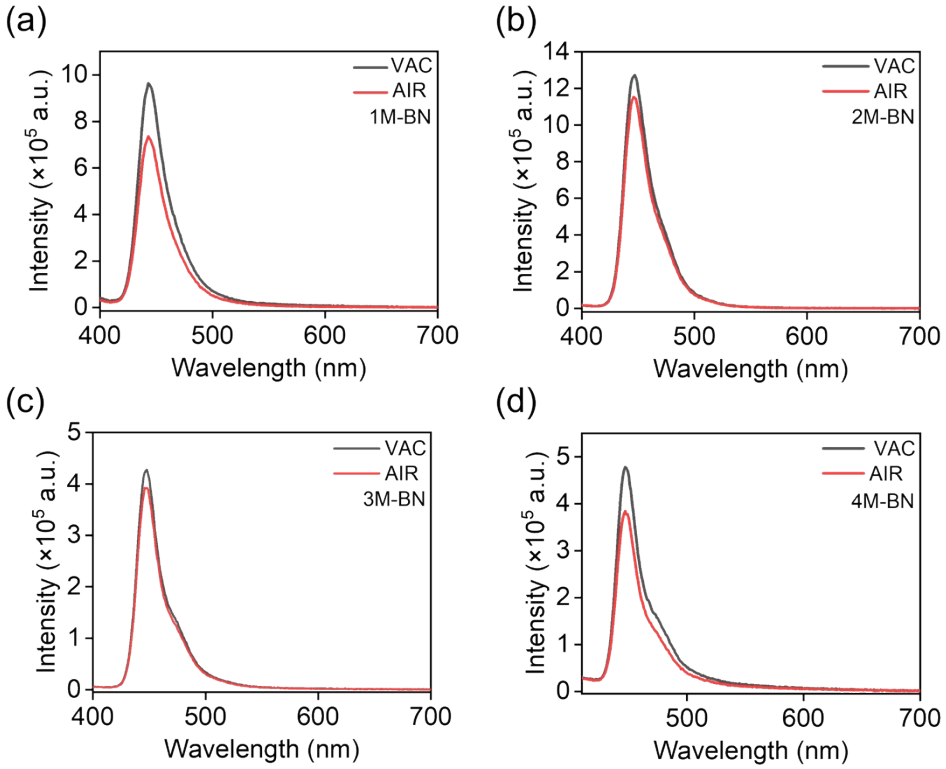

Figure S24. Temperature-dependent transient PL decay spectra of (a) 1M-BN, (b) 2M-BN, (c) 3M-BN and (d) 4M-BN (1 wt% in mCBP doped films).

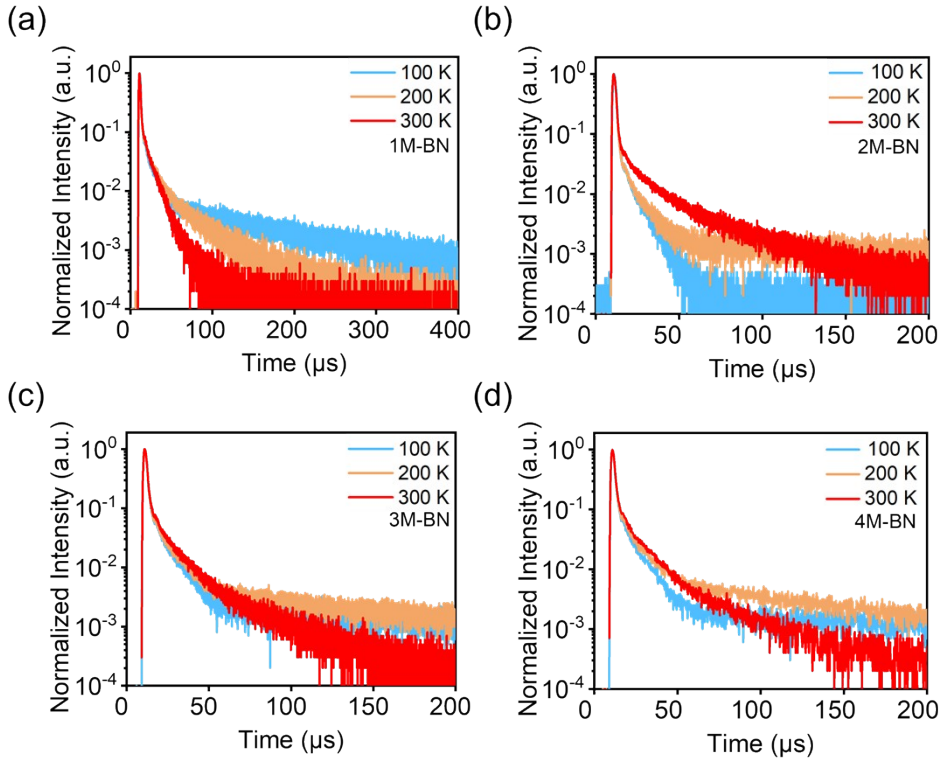

Figure S25. Temperature-dependent transient PL decay spectra of (a) 1M-BN, (b) 2M-BN, (c) 3M-BN and (d) 4M-BN (1 wt% in mCBP doped films).

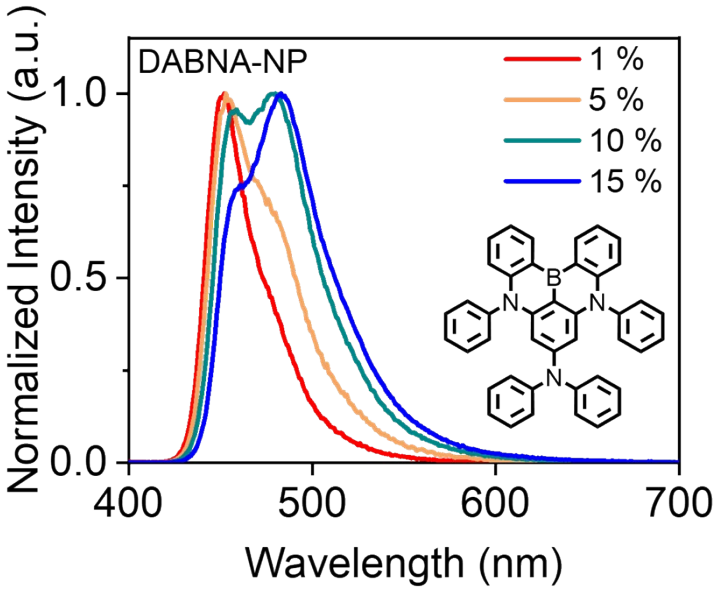

Figure S26. Steady-state PL spectra measured at 300K for the doped films of DABNA-NP in doped films (1 wt%, 5 wt%, 10 wt% and 15 wt% in mCBP).

Table S2. PLQYs and FWHMs of DABNA-NP at a doping concentration range of 1-15 wt%.

Doping Conc. [wt %]	PLQY [%]	FWHM [nm]
1	94	32
5	85	37
10	80	60
15	51	62

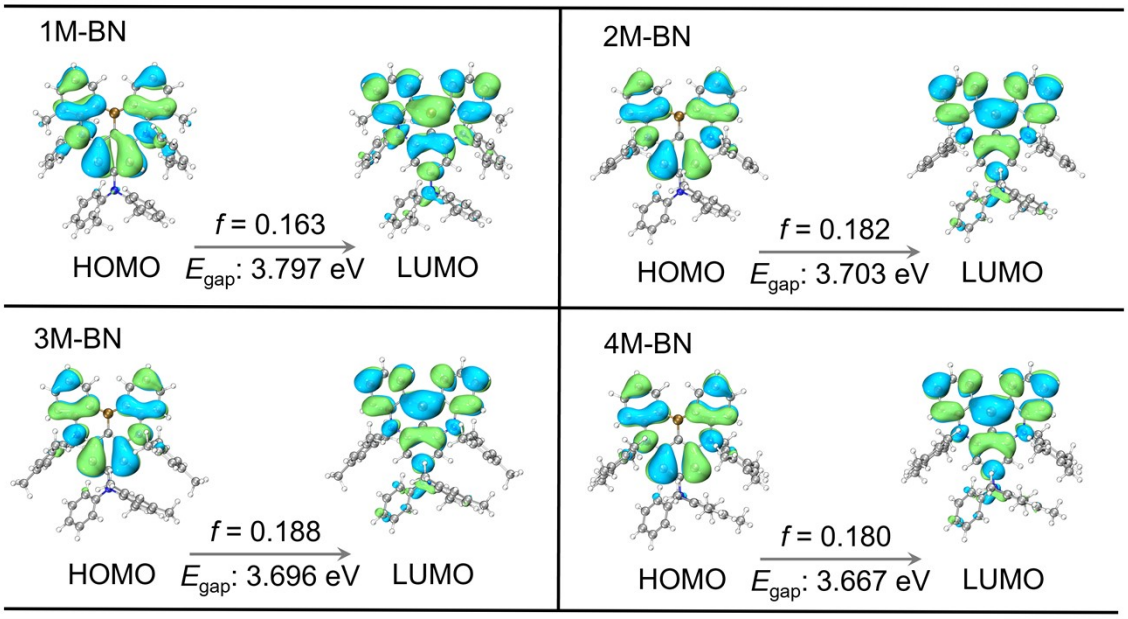

Figure S27. HOMO and LUMO distributions (isosurface = 0.02), energy gap (E_{gap}) and oscillator strengths (f) of 1M-BN, 2M-BN, 3M-BN and 4M-BN.

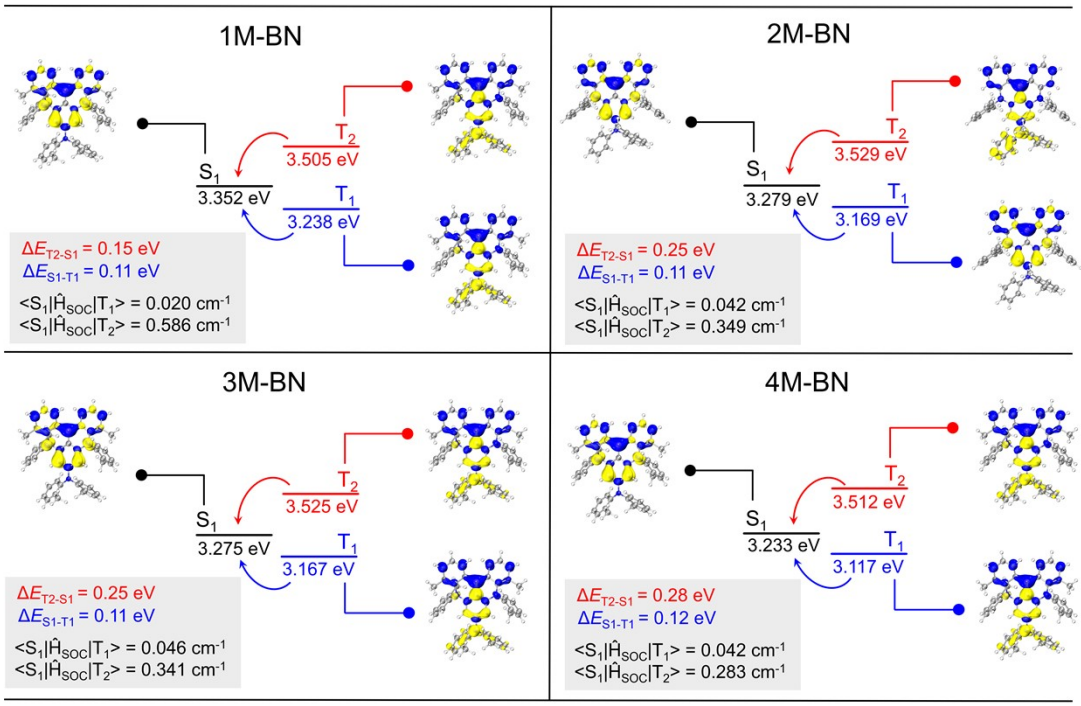

Figure S28. NTOs, ΔE_{ST}s and SOC contants of four emitters for S_1, T_1 and T_2 states.

The non-monotonic variation of k_{RISC} across the series reflects a delicate balance between electronic coupling and structural rigidity. Although **1M-BN** exhibits more favorable $T_2 \rightarrow S_1$ parameters, including larger SOC and smaller $\Delta E_{S1\text{-}T2}$, these advantages are offset by its weaker direct $T_1 \rightarrow S_1$ coupling and lower PLQY, resulting in a k_{RISC} comparable to that of **2M-BN**. In contrast, the slightly reduced SOC matrix elements of **3M-BN** and **4M-BN** further diminish their k_{RISC} values, which limit efficient spin-flip transitions. Overall, despite these variations, all four emitters exhibit relatively small and similar k_{RISC} values. This behavior is primarily governed by the intrinsic planarity of the MR core, while peripheral methyl substitution serves only to fine-tune the excited-state dynamics.

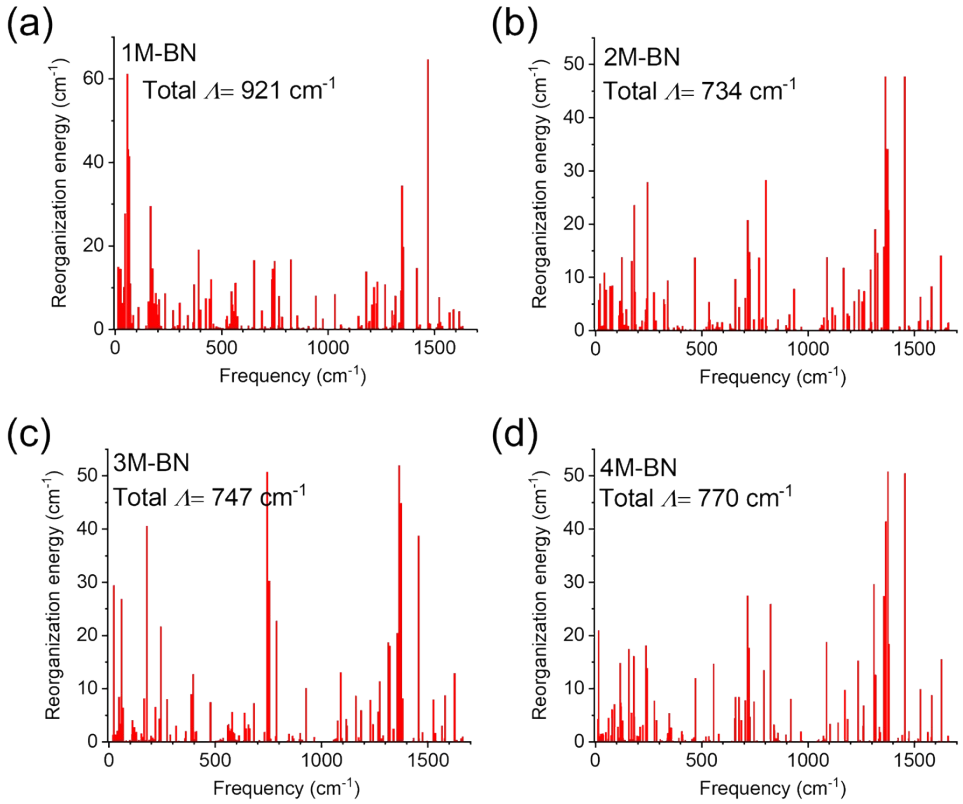

Figure S29. The $S_1 \rightarrow S_0$ reorganization energy (Λ_{reorg}) of (a) 1M-BN, (b) 2M-BN, (c) 3M-BN and (d) 4M-BN.

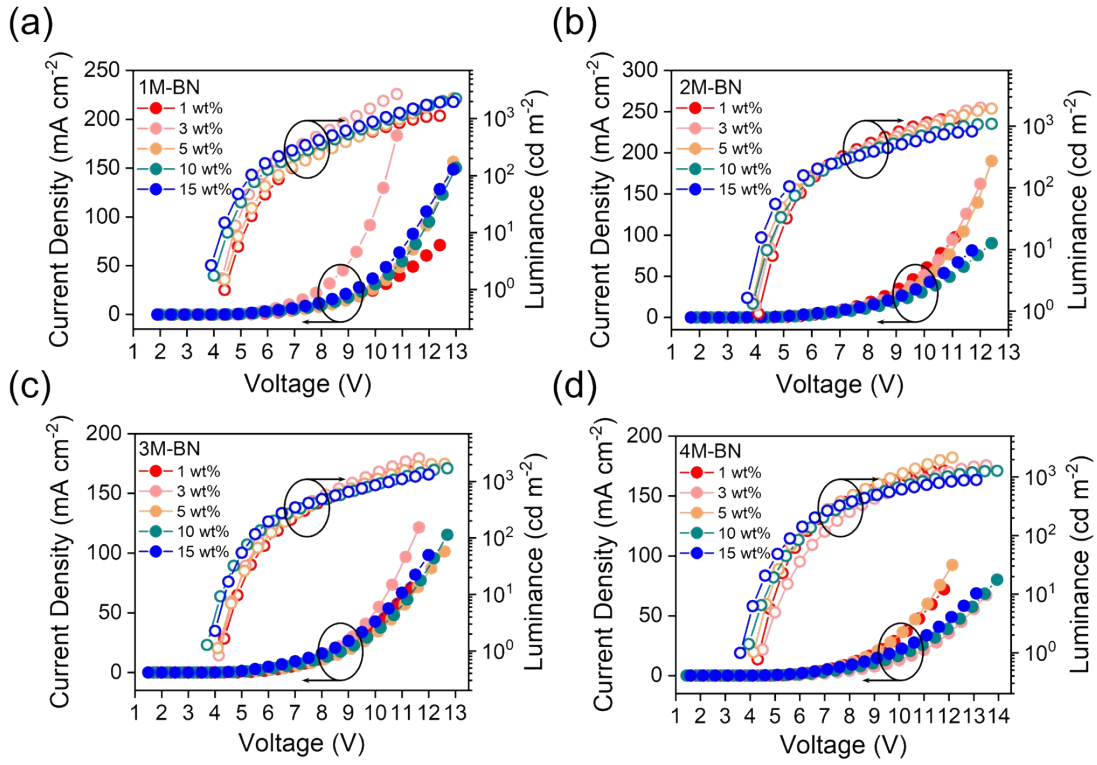

Figure S30. Current density and luminance versus voltage curves of 1M-BN (a), 2M-BN (b), and 3M-BN (c) and 4M-BN (d) at different doping concentrations.

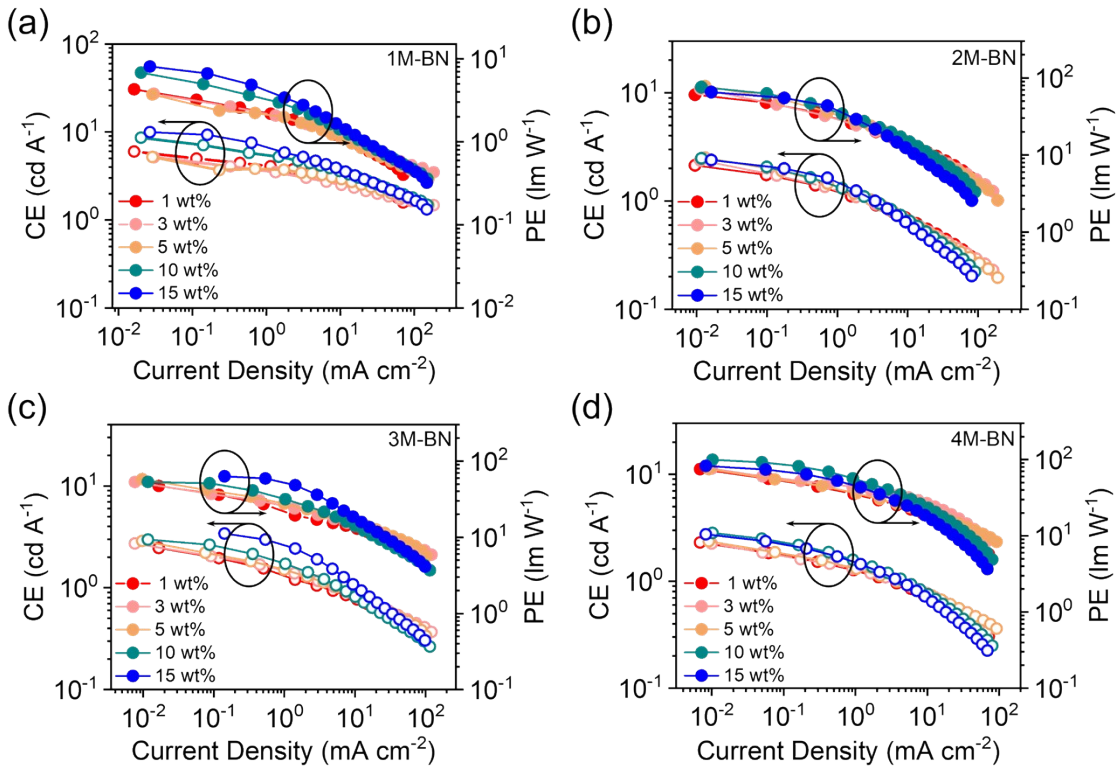

Figure S31. Current efficiency/power efficiency-current density curves of (a) 1M-BN, (b) 2M-BN, (c) 3M-BN and (d) 4M-BN based OLED at different doping concentrations.

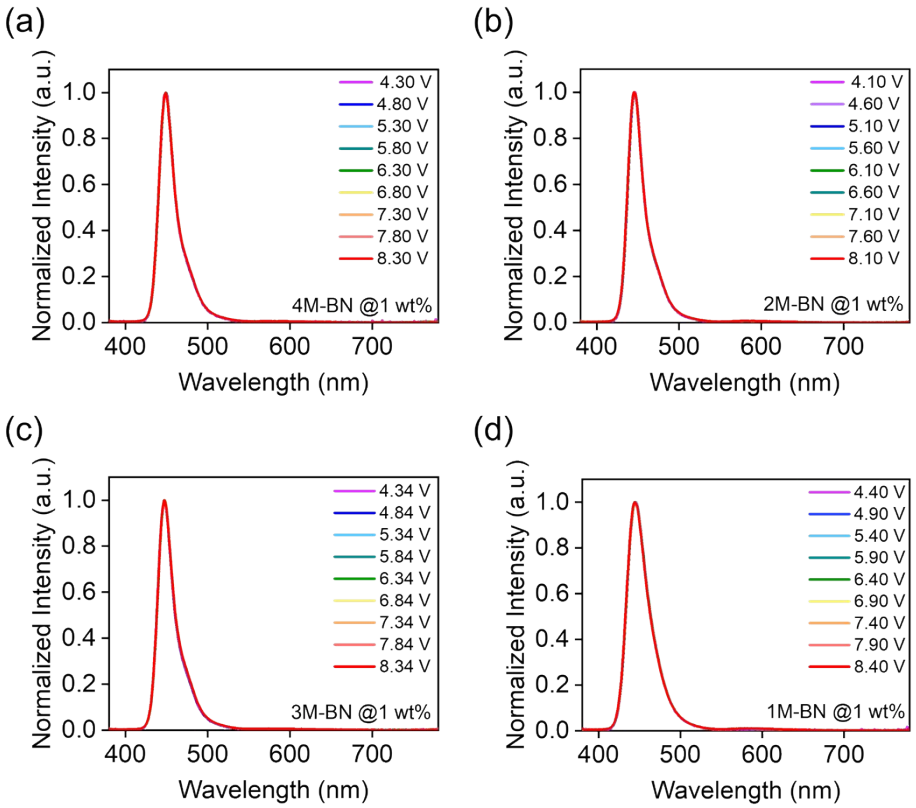

Figure S32. EL spectra of 1M-BN, 2M-BN, 3M-BN and 4M-BN based OLED at 1 wt% doping concentrations from ~4V to ~8.5V.

Table S3. Summary of the deep-blue MR-TADF based OLEDs with CIE_y < 0.046 in recent years.

Com.	Concentration-independent	λ_{EL}[c] [nm]	FWHM[d] [nm]	EQE_{max}[f] [%]	CIE[g] [x, y]	Ref.
1M-BN	Yes	445	31	13.3	0.155, 0.045	This work
2M-BN		447	22	26.9	0.152, 0.045	
3M-BN		448	23	22.1	0.153, 0.046	
2B-DTACrs	No	447	26	14.8	0.150, 0.044	Chem. Commun., 2022, 58, 9377-9380
BOBO-Z	No	445	18	13.6	0.15,0.04	Adv. Mater., 2022, 34, 2107951
IPrBN-mCP	Yes	451	20	33.4	0.146, 0.046	Adv. Funct. Mater., 2025, 35, 2414635
3BON	Yes	443	24	24.8	0.155, 0.045	Angew. Chem. Int. Ed., 2025, 64, e202518651
DBMes	No	440	19	13.1	0.158, 0.024	Chem. Eng. J., 2025, 516, 164225
2	No	442	27	11.0	0.153, 0.036	Angew. Chem. Int. Ed., 2025, 64, e202510891
3		441	25	9.1	0.155, 0.030	
4		441	25	8.1	0.154, 0.040	
6		408	29	1.5	0.160, 0.026	
DBNO	No	447	25	27.2	0.149, 0.042	Chem. Sci., 2025, 16,

DMBNO	Yes	449	25	32.3	0.148, 0.046	3655-3661
Py-BN	No	444	21	15.8	0.153, 0.046	Angew. Chem. Int. Ed., 2024, 63, e202408522
Pm-BN		415	24	5.8	0.161, 0.045	
TBNO-2	No	452	17	40.4	0.142, 0.044	Adv. Mater. 2025, e17512

Supplementary references

1 M. Quan, Z.-L. Zhu, G. Chen, J. Miao and C. Yang, *Angew. Chem. Int. Ed.*, 2025, **64**, e202512162.

2 Z. Liu, T. Lu and Q Chen, *Carbon*, 2020, **165**, 461-467.

3 T. Lu and F. Chen, *J. Comput. Chem.*, 2011, **33**, 580-592.

4 M. Kállay, P. R. Nagy, D. Mester, Z. Rolik, G. Samu, J. Csontos, J. Csóka, P. B. Szabó, L. Gyevi-Nagy, B, Hégely, I, Ladjánszki, L. Szegedy, B. Ladóczki, K. Petrov, M. Farkas, P. D. Mezei and Á. Ganyecz, *J. Chem. Phys.*, 2020, **152**, 074107.